IVYSPRING INTERNATIONAL PUBLISHER

Theranostics

2018; 8(7): 1966-1984. doi: 10.7150/thno.23848

Research Paper

Dual Chemodrug-Loaded Single-Walled Carbon Nanohorns for Multimodal Imaging-Guided Chemo-Photothermal Therapy of Tumors and Lung Metastases

Jingxing Yang[1, 2], Huilan Su[3], Wenshe Sun[1, 2], Jiali Cai[4], Shiyuan Liu[4], Yimin Chai[1], Chunfu Zhang[1, 2]✉

1. Shanghai Jiao Tong University Affiliated 6th Hospital, School of Biomedical Engineering, Shanghai Jiao Tong University, Shanghai 200030, China.
2. Department of Nuclear Medicine, Rui Jin Hospital, School of Medicine, Shanghai Jiao Tong University, Shanghai 200030, China.
3. State Key Laboratory of Metal Matrix Composites, School of Materials Science and Engineering, Shanghai Jiao Tong University, Shanghai 200240, China
4. Changzheng Hospital, Secondary Military Medical University, Shanghai 200003, China.

✉ Corresponding author: Tel: 0086-21-62933323; Fax: 0086-21-62933323; E-mail: cfzhang@sjtu.edu.cn

Received: 2017.11.14; Accepted: 2018.01.21; Published: 2018.02.15

Abstract

Tumor combination therapy using nano formulations with multimodal synergistic therapeutic effects shows great potential for complete ablation of tumors. However, targeting tumor metastases with nano structures is a major obstacle for therapy. Therefore, developing a combination therapy system able to target both primary tumors and their metastases at distant sites with synergistic therapy is desirable for the complete eradication of tumors. To this end, a dual chemodrug-loaded theranostic system based on single walled carbon nanohorns (SWNHs) is developed for targeting both primary breast tumors and their lung metastases.

Methods: SWNHs were first modified simultaneously with poly (maleic anhydride-alt-1-octadecene) (C_{18}PMH) and methoxypolyethyleneglycol-b-poly-D, L-lactide (mPEG-PLA) *via* hydrophobic–hydrophobic interactions and π-π stacking. Then cisplatin and doxorubicin (DOX) (2.9:1 molar ratio) were sequentially loaded onto the modified nanohorns in a noninterfering way. After careful examinations of the release profiles of the loaded drugs and the photothermal performance of the dual chemodrug-loaded SWNHs, termed SWNHs/C_{18}PMH/mPEG-PLA-DOX-Pt, the dual drug chemotherapeutic and chemo-photothermal synergetic therapeutic effects on tumor cells were evaluated. Subsequently, the *in vivo* behavior and tumor accumulation of the drug-loaded SWNHs were studied by photoacoustic imaging (PAI). For chemo-photothermal therapy of tumors, 4T1 tumor bearing mice were intravenously injected with SWNHs/C_{18}PMH/mPEG-PLA-DOX-Pt at a dose of 10 mg/kg b.w. (in SWNHs) and tumors were illuminated by an 808 nm laser (1W/cm^2 for 5 min) 24 h post-injection.

Results: DOX and cisplatin were loaded onto the modified SWNHs with high efficiency (44 wt% and 66 wt%, respectively) and released in a pH-sensitive, tandem and sustainable manner. The SWNHs/C_{18}PMH/mPEG-PLA-DOX-Pt had a hydrodynamic diameter of 182 ± 3.2 nm, were highly stable in physiological environment, and had both dual drug chemotherapeutic (CI = 0.439) and chemo-photothermal synergistic antitumor effects (CI = 0.396) *in vitro*. Moreover, the dual drug-loaded SWNHs had a long blood half-life (10.9 h) and could address both the primary breast tumors and their lung metastases after intravenous administration. Consequently, chemo-photothermal combination therapy ablated the primary tumors and simultaneously eradicated the metastatic lung nodules.

Conclusion: Our study demonstrates that SWNHs/C_{18}PMH/mPEG-PLA-DOX-Pt is highly potent for chemo-photothermal combination therapy of primary tumors and cocktail chemotherapy of their metastases at a distant site.

Key words: Single walled carbon nanohorns, Photoacoustic imaging, Chemo-photothermal therapy, Tumor metastasis

Introduction

Chemotherapy is a major cancer treatment strategy [1-3]. However, mono-drug chemotherapy has limitations in clinical practice, such as drug resistance, systemic toxicity and tumor recurrence [4, 5]. To overcome these limitations, combination chemotherapy, the simultaneous administration of multiple therapeutic agents, has been routinely exploited and implemented in the clinic [6, 7]. Unlike monotherapy, combination chemotherapy can modulate different signaling pathways in cancer cells, elicit synergetic responses and maximize the therapeutic effect [8, 9]. For instance, doxorubicin (DOX) and cisplatin can produce a synergetic anticancer effect *via* distinct interference of DNA activity. Cisplatin can covalently bind to DNA purine bases, forming intra- or inter-strand cross-links on DNA, thus inhibiting its cellular transcription and triggering tumor cell apoptosis [10], while DOX binds to DNA-associated enzymes, intercalates with DNA base pairs, and targets multiple molecular targets to produce a range of cytotoxic effects [11]. Indeed, the co-administration of DOX with cisplatin has been shown to improve the therapeutic efficacy in different types of cancers [8, 9, 12-14]. However, the administration of combination regimens as drug cocktails is frequently associated with varying pharmacokinetics and a lack of site-specific accumulation and delivery of the drugs [8, 15, 16]. Moreover, to achieve the optimal synergistic effect, the ratio of co-administration drugs is also a key factor. For example, CPX-351, a liposomal formulation of daunorubicin and cytarabine demonstrated an optimized synergistic therapeutic effect on acute myelocytic leukemia (AML) in clinical at a 1:5 molar ratio (corresponding to 5 mg/kg cytarabine and 2.2 mg/kg daunorubicin) [17]. Therefore, it is highly desirable, albeit challenging, to rationally design an appropriate drug carrier to achieve simultaneous multi-drug loading, unify the pharmacokinetics of each drug, achieve targeted delivery, and thus realize the maximum synergistic effect of the loaded drugs with minimal side effects. With progress in cancer theranostics in recent years, nanomaterials have demonstrated many advantages as drug carriers, including better drug solubility, improved pharmacokinetic and pharmacodynamic properties, minimized side effects, and site-specific delivery through the enhanced permeability and retention (EPR) effect [18, 19]. Moreover, it has been reported that thermal treatment can largely augment cocktail chemotherapeutic efficacy and trigger an autoimmune response [20, 21]. Therefore, the combination of photothermal therapy (PTT) along with therapeutic agents has recently attracted extensive attention in the field of cancer treatment [22, 23]. In this context, drug delivery systems based on PTT agents have been intensively explored, but most have only loaded single hydrophilic or hydrophobic drugs [24]. Multidrug delivery systems have also been developed, but some have exhibited a relatively low loading efficiency because the loading of one drug frequently reduced the quantity of another drug [25]. Moreover, owing to the complicated structures of these systems, their fabrication is often complex. Therefore, it is desirable to develop a readily prepared nano-vehicle that can efficiently load multiple chemotherapeutic agents (e.g., DOX and cisplatin) while simultaneously serving as a PTT agent.

Since the major tissue chromophores and blood show minimum absorption in the near-infrared (NIR) range (650–900 nm) [26], nanomaterials such as gold nanorods, cages, and spheres [22, 27]; carbonaceous nanomaterials [28, 29]; and polymeric nanostructures [21, 30] with good absorption in this spectral region have been widely explored for PTT. Among various carbonaceous materials, single-walled carbon nanohorns (SWNHs) are advantageous for drug loading and have strong potential for chemo-photothermal combination therapy owing to their unique structure and properties. A SWNH is a horn-shaped, single-walled graphitic tubule with a conical tip of 2–5 nm in diameter and 40–50 nm in length [31]. This closed-tip nanotube possesses larger inner voids and can be filled with suitable drugs ranging from small molecules to proteins. SWNHs do not exist individually but ~2,000 SWNHs assemble, through van der Waals forces, to form a "dahlia"-like aggregate with a diameter of about 50–100 nm, which is expected to exert an enhanced EPR effect that makes SWNHs effective for the passive delivery of drugs to tumors [32, 33]. In addition to this, SWNHs have high purity and are free of toxic metallic impurities, making them biocompatible and safe for *in vivo* application. Furthermore, SWNHs have strong absorption in the NIR region (700-900 nm), with a high photo-thermal conversion efficiency, thus positioning them as a suitable candidate for PTT [5, 34].

Moreover, photoacoustic imaging (PAI), a high spatial resolution and deep bio-tissue penetration imaging technology, can offer three-dimensional images of tumor tissues in preclinical research and clinical applications [35, 36]. Because the acoustic signal is generated by thermal expansion, SWNHs might also be viable photoacoustic contrast agents, thus allowing real-time monitoring of the delivery of therapeutic agents to the tumor site and offering visible guidance in PAI-mediated cancer therapy [37].

Therefore, in the present study, we rationally designed and fabricated a highly potent chemo-photothermal theranostic system by sequentially loading DOX and cisplatin onto dual polymer-modified SWNHs (Scheme 1). The dual chemodrug-loaded system, termed SWNHs/C_{18}PMH/mPEG-PLA-DOX-Pt, exhibited a pH-responsive, tandem, and sustainable drug release and showed high accumulation in both primary tumors and their metastases through the EPR effect. As a result, chemo-photothermal combination therapy guided by PAI completely ablated primary tumors and simultaneously eradicated their metastases in the lung.

Results and Discussion

Synthesis and Characterization of Dual Chemodrug-Loaded SWNHs

The pristine SWNHs were hydrophobic with an average diameter of 77.2 ± 14.3 nm (Figure 1A) and a specific surface area of ~281 m^2/g (Figure S1). The hydrophobic SWNHs were simultaneously modified with poly (maleic anhydride-alt-1-octadecene) (C_{18}PMH, MW 1051 Da) and methoxypolyethylene-glycol-b-poly-D, L-lactide (mPEG-PLA, MW 5K-5K Da) by assembling their hydrophobic sections with SWNHs in the aqueous media through hydrophobic–hydrophobic interactions, leaving the hydrophilic moieties (maleic anhydride and mPEG) extending externally. After modification, the average hydrodynamic size and zeta potential of the obtained nanohorns (designated as SWNHs/C_{18}PMH/mPEG-PLA) were 130 ± 1.2 nm (Figure 1B) and −34.7 ± 1.8 mV (Table S1), respectively. SWNHs/C_{18}PMH/mPEG-PLA was highly stable under physiological conditions and no precipitates were observed following centrifugation at a speed of 12,857 ×g for 1 h (Figure S2).

Next, DOX and cisplatin were sequentially loaded onto the modified SWNHs. As shown in Table S2, the drug-loading capacity (DLC) of DOX on 0.5 mg of SWNHs/C_{18}PMH/mPEG-PLA (1 mL) steadily increased with increasing DOX concentration, with a high drug-loading efficiency (DLE, >80%) at each concentration investigated. Next, cisplatin was loaded onto the DOX-loaded SWNHs/C_{18}PMH/mPEG-PLA (SWNHs/C_{18}PMH/mPEG-PLA-DOX). Separate from DOX loading, the DLC of cisplatin on the same amount of modified SWNHs increased initially and then plateaued with further increases in cisplatin concentration, while the DLE gradually decreased. It has been reported that a higher cisplatin/DOX-loading molar ratio could produce a better synergetic chemotherapeutic effect at a lower drug concentration [14]. Therefore, cisplatin and DOX at the maximum molar ratio of 2.9 were loaded for the following studies, corresponding to 0.22 mg of DOX and 0.33 mg of cisplatin loaded onto 0.5 mg of modified SWNHs. The different loading profiles of DOX and cisplatin may arise from their distinct loading mechanisms. DOX loading can be achieved *via* hydrophobic–hydrophobic interactions and a π–π stacking interaction between the anthraquinone ring of DOX and the SWNHs, similar to that observed for single-walled carbon nanotubes (SWCNT), multi-walled carbon nanotubes (SMWCNT), graphene oxide (GO), and fullerenes [38-42]. Cisplatin loading, however, was through the coordination of $[(NH_2)_2Pt(H_2O)_2]^{2+}$ with carboxylic groups from the hydrolyzed anhydride in C_{18}PMH [43, 44]. When the carboxylic groups in the modification layer were consumed, cisplatin loading would saturate. After cisplatin loading, the zeta potential of the dual drug-loaded SWNHs, designated as SWNHs/C_{18}PMH/mPEG-PLA-DOX-Pt, was −14.0 ± 1.1 mV (Table S1). Transmission electron microscopy (TEM) images revealed that SWNHs/C_{18}PMH/PLA-PEG-DOX-Pt were relatively monodisperse (Figure 1C). The average hydrodynamic size of SWNHs/C_{18}PMH/PLA-PEG-DOX-Pt was 182 ± 3.2 nm, and the system was

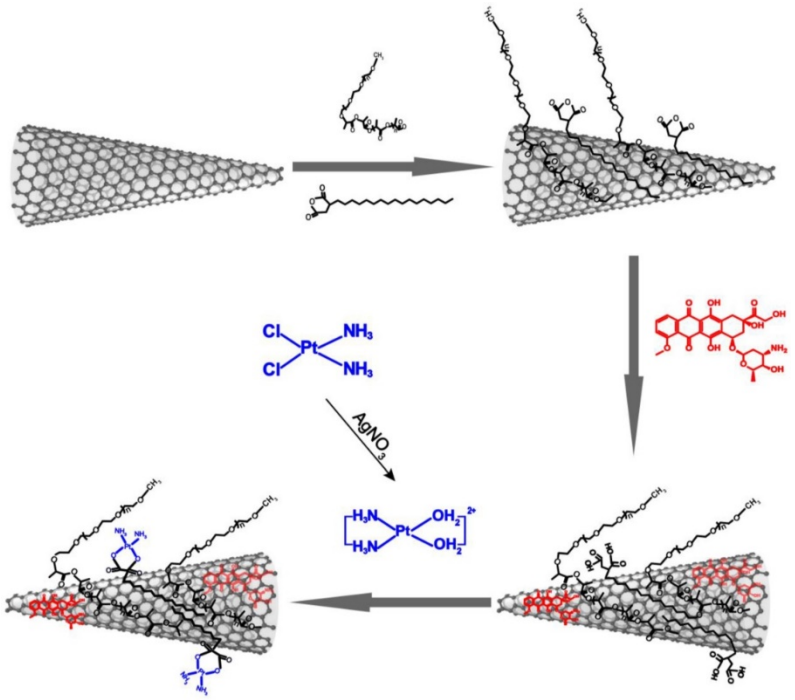

Scheme 1. Schematic illustration of the preparation of dual drug-loaded SWNHs.

highly stable under physiological conditions (RPMI-1640 cell culture media with 10% fetal bovine serum (FBS); Figure 1D). In addition, single drug-loaded SWNHs containing either DOX or cisplatin at the same loading capacity as that used for dual drug-loaded SWNHs, termed SWNHs/C_{18}PMH/PLA-PEG-DOX and SWNHs/C_{18}PMH/PLA-PEG-Pt, respectively, were also prepared and characterized as controls.

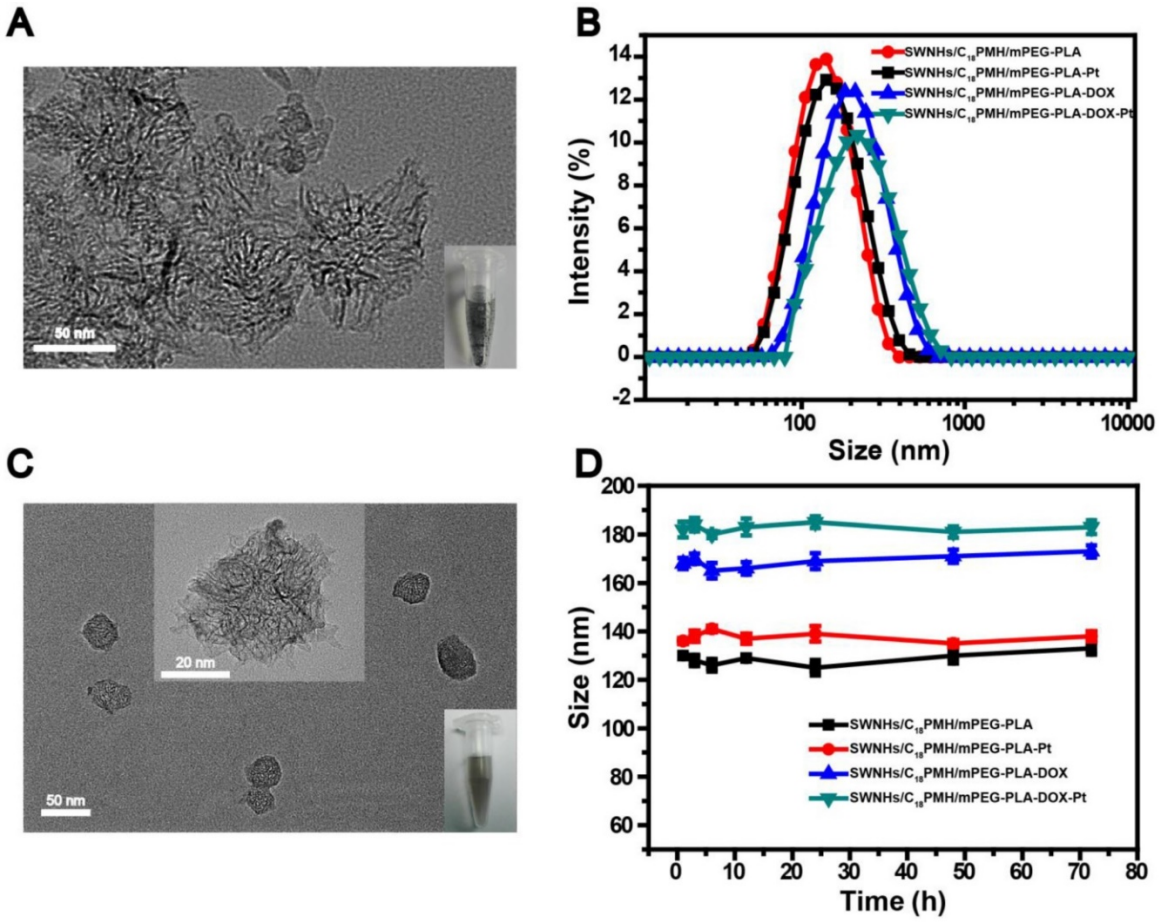

Figure 1. Characterization of drug-free and the drug-loaded SWNHs. A, C) Transmission electron microscopy image of pristine SWNHs (A) and SWNHs/C_{18}PMH/mPEG-PLA-DOX-Pt (C). Insets show the solubility of SWNHs in PBS before modification and after drug loading. B, D) Size distribution and stability of modified and drug-loaded SWNHs in RPMI-1640 medium.

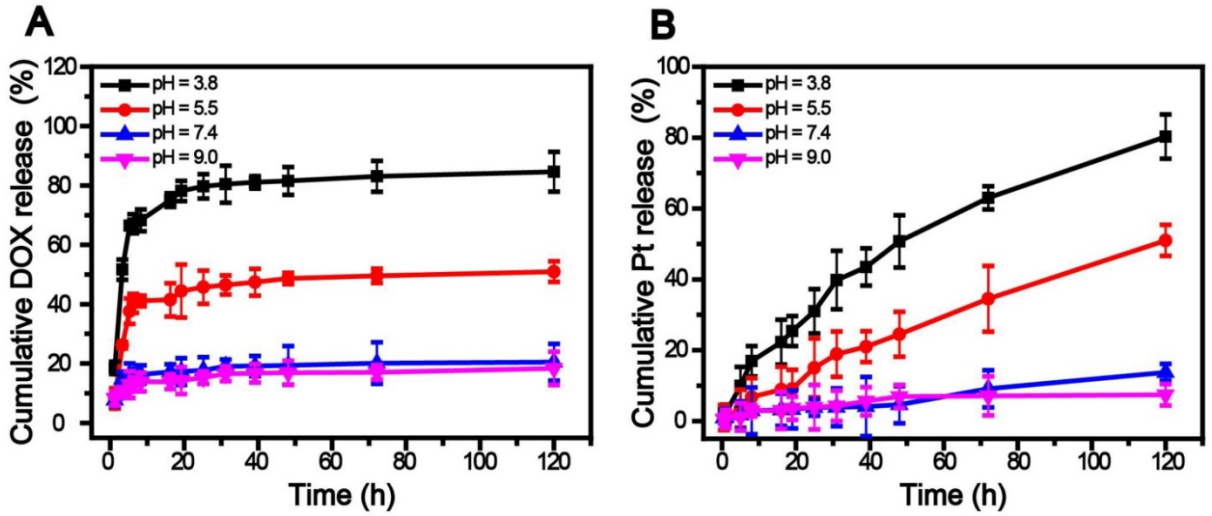

Figure 2. A, B) Release profiles of DOX and cisplatin from SWNHs/C_{18}PMH/mPEG-PLA-DOX-Pt at various pH values and 37 °C.

Drug Release

The release of DOX and cisplatin was studied by suspending SWNHs/C_{18}PMH/mPEG-PLA-DOX-Pt in phosphate buffered saline (PBS) at different pH levels at 37 °C. As shown in Figure 2, both DOX and cisplatin exhibited pH-sensitive release behavior. However, DOX release was more rapid and culminated in a relatively short term. The cumulative release within 6 h was determined to be 67.12%, 40.31%, 15.82%, and 13.05% at pH values of 3.8, 5.5, 7.4, and 9.0, respectively. The release might have been triggered by the reduction in π–π linkages between DOX and SWNHs in acidic media while being stable under neutral and alkaline conditions [45]. In contrast, cisplatin release was more sustainable under the same conditions. Compared with DOX, the cumulative release within 6 h was only 12.13% and 3.86% at pH 3.8 and 5.5, respectively, and negligible at pH 7.4 (2.14%) and 9.1 (1.58%). The slower release of cisplatin may have resulted from its immobilization onto the nanohorns *via* strong coordination bonds. At a pH similar to the intracellular microenvironment (pH = 5.5) [46, 47], 45.75% of DOX and 15.14% of cisplatin was released over 24 h. It has been reported that tumor cells develop drug resistance during chemotherapy with DOX [8, 9] and the DOX-resistant cells might be killed by cisplatin subsequently released from SWNHs/C_{18}PMH/mPEG-PLA-DOX-Pt [8, 12, 14]. Therefore, the tandem release of DOX and cisplatin might be favorable for cancer therapy: once the nanocarriers are taken up by cancer cells, the system can rapidly respond to tumors in a sustained manner [46, 47].

Interestingly, it was observed that the UV-Vis signal of DOX at 480 nm was quenched after the drug was loaded onto SWNHs and recovered once released (Figure S3). The quenching of DOX fluorescence signal was caused by the strong absorption of SWNHs, leading to energy transfer from DOX to SWNHs [48, 49]. A similar phenomenon has also been observed when DOX was loaded on PAA-Co_9Se_8 nanoplates [23], multi-walled carbon nanotube [42, 48] and graphene oxide [49]. This phenomenon generated a switch-on fluorescence signal at the tumor site upon the release of DOX from SWNHs at acidic pH, thus providing a flexible method to observe the cellular uptake of SWNHs (Figure S4).

Photothermal Conversion Performance

Next, we evaluated the photothermal performance of the dual drug-loaded SWNHs by illuminating a water suspension of the system (400 μL) at a concentration of 50 μg/mL using an 808 nm laser at different laser power densities, or various concentrations (0-100 μg/mL) with a fixed laser power density of 1 W/cm^2. The temperature of the suspensions was monitored using a digital thermometer with a thermocouple probe submerged in the solution. As shown in Figure 3A and B, the photothermal conversion performance was dependent on laser power, SWNH concentration, and irradiation time, similar to other photothermal agents frequently reported [22, 23, 38, 42]. When the concentration of SWNHs/C_{18}PMH/mPEG-PLA-DOX-Pt was 50 μg/mL with irradiation at a laser power of 2 W/cm^2 for 10 min, the temperature of the suspension reached as high as 86.9 °C, significantly higher than that required for tumor ablation [22, 23, 50]. More significantly, the SWNHs/C_{18}PMH/mPEG-PLA-DOX-Pt system was shown to be thermostable. Following six cycles of laser on/off tests and irradiation at a power density of 1 W/cm^2 for 5 min (300 J/cm^2) with a SWNH concentration of 50 μg/mL (Figure 3C and D), the temperature of the resultant suspension could recover to the initial value (64.4 ± 0.6 °C), and no aggregates were subsequently observed. The characteristics of these dual drug-loaded SWNHs allowed optimal temperature elevation by adjusting SWNH concentration, laser power density, or illumination time to maximize the effect on tumor ablation.

In Vitro Cytotoxicity of Dual Drug-Loaded Nanohorns

Synergetic Chemotherapy with SWNHs/C_{18}PMH/mPEG-PLA-DOX-Pt

To evaluate the chemotherapeutic effect of the dual drug-loaded SWNHs, 4T1 cells, a murine breast cancer cell line with a high rate of recurrence and metastasis [51, 52], were seeded into 96-well plates and treated with SWNHs/C_{18}PMH/mPEG-PLA, SWNHs/C_{18}PMH/mPEG-PLA-DOX, SWNHs/C_{18}PMH/mPEG-PLA-Pt, or SWNHs/C_{18}PMH/mPEG-PLA-DOX-Pt at different doses (by SWNHs) for 24 h. After treatment, cell viability was evaluated by cell count kit-8 (CCK-8) assay (Figure 4A). SWNHs/C_{18}PMH/mPEG-PLA alone did not exhibit an obviously cytotoxic effect, which may be attributable to the unique catalyst-free preparation of SWNHs [53]. However, both dual and single drug-loaded SWNHs demonstrated dose-dependent cytotoxicity. SWNHs/C_{18}PMH/mPEG-PLA-DOX-Pt and SWNHs/C_{18}PMH/mPEG-PLA-DOX significantly induced cell death at a dose as low as 1 μg/mL, with SWNHs/C_{18}PMH/mPEG-PLA-DOX-Pt being more potent (cell viability: 73.0% ± 2.9% vs. 88.5% ± 7.5%, $p < 0.001$). For cisplatin-loaded SWNHs (SWNHs/C_{18}PMH/mPEG-PLA-Pt), significant cell death was

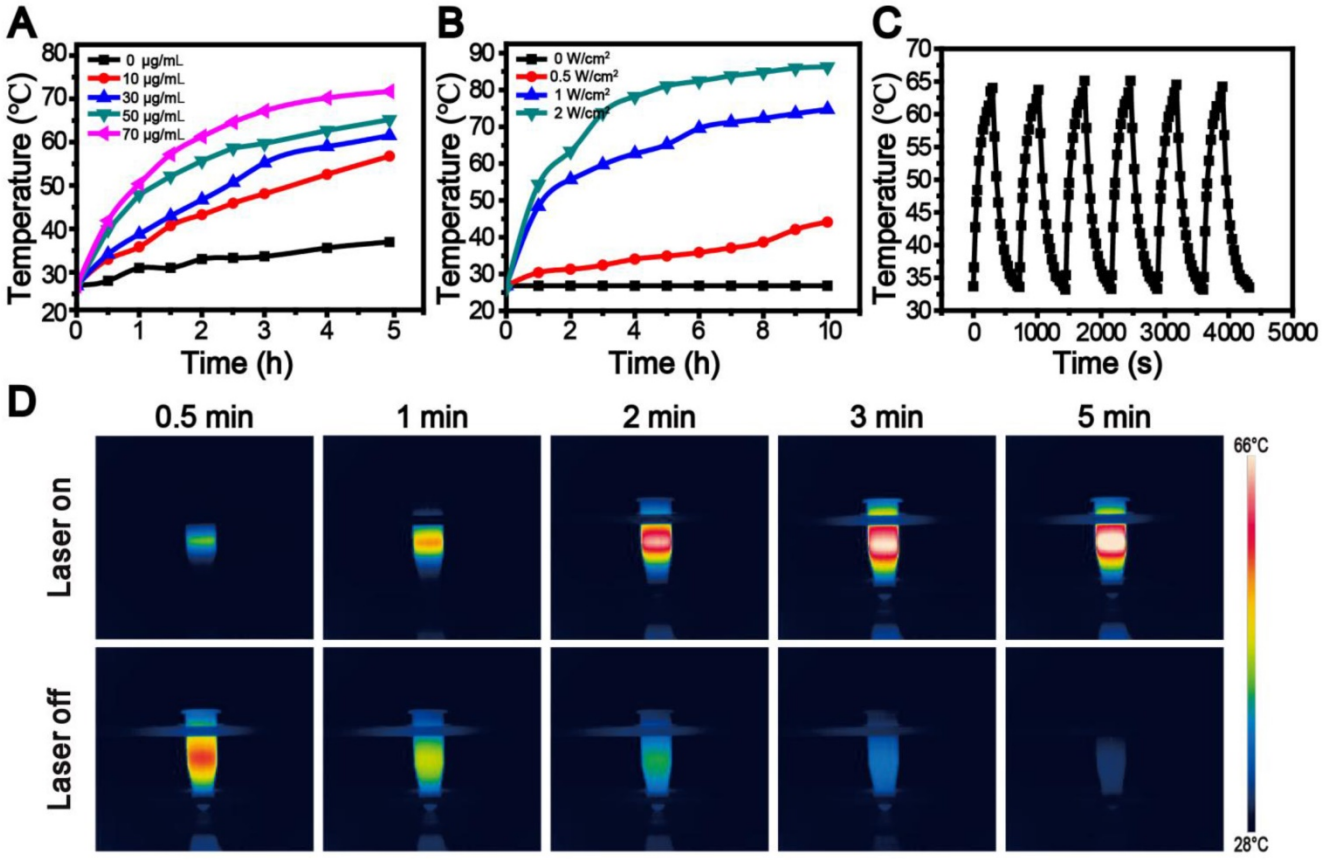

Figure 3. Photothermal performance of SWNHs/C_{18}PMH/mPEG-PLA-DOX-Pt. A, B) Temperature elevation curves of SWNHs/C_{18}PMH/mPEG-PLA-DOX-Pt suspensions at a concentration of 50 μg SWNHs/mL, exposed to an 808 nm laser at various power densities (A) or various concentrations exposed to 1 W/cm² (B). C) Real-time temperature measurement of SWNHs/C_{18}PMH/mPEG-PLA-DOX-Pt suspensions (50 μg SWNHs/mL, 400 μL) under cycle laser irradiation (1 W/cm²) for six cycles. Each cycle consisted of 5 min irradiation followed by a cooling phase. D) Thermographic images of SWNHs/C_{18}PMH/mPEG-PLA-DOX-Pt (50 μg SWNHs/mL) in centrifuge tubes after 808 nm laser irradiation at 1 W/cm² for 5 min (upper row) and recovery at room temperature with the laser off for a further 5 min (lower row).

observed at a dose of 5 μg/mL (cell viability: 79.7% ± 5.3%). These observations indicated that the dual drug-loaded SWNHs were more potent than the single drug-loaded system, and that SWNHs loaded with DOX were more effective than those loaded with cisplatin at a relatively lower concentration. Indeed, the IC_{50} (half-maximal inhibitory concentration) values of SWNHs/C_{18}PMH/mPEG-PLA-DOX, SWNHs/C_{18}PMH/mPEG-PLA-Pt, and SWNHs/C_{18}PMH/mPEG-PLA-DOX-Pt were 3.01, 3.78, and 1.37 μg/mL, respectively, which were 1.4-, 1.9-, and 1.4-fold lower than the free DOX, cisplatin, and DOX/cisplatin combination (Figure S5). To illustrate the mechanism of the loaded drug effect on tumor cell viability, the combination index (CI), equal to $C_1/C_{x1} + C_2/C_{x2}$, was calculated [9, 14]. The CI value of the dual drug-loaded SWNHs was 0.439, which indicated a synergistic therapeutic effect. These observations were consistent with previous findings that cocktail chemotherapy with DOX and cisplatin has a synergetic therapeutic effect on cancer cells [9, 14, 54, 55]. Because DOX is released more rapidly than cisplatin (24 h at pH 5.5: 45.75% ± 5.61% vs. 15.14% ± 8.30%), it is reasonable to suggest that SWNHs/C_{18}PMH/mPEG-PLA-DOX were more effective at cell killing than SWNHs/C_{18}PMH/mPEG-PLA-Pt at a relatively lower concentration. At a higher drug concentration (50 μg/mL), however, the difference in tumor cell killing between single and dual drug-loaded SWNHs was marginal.

To further illustrate the synergetic therapeutic effect of the dual drug-loaded SWNHs, 4T1 cells were treated with single or dual drug-loaded SWNHs at a dosage of 10 μg/mL (DOX = 4.4 μg/mL; cisplatin = 6.6 μg/mL) for 24 h. Subsequently, the culture media was removed, and the cells were maintained in fresh media for another 24 h. As shown in Figure 4B, cell viability was decreased compared with that of cells evaluated immediately after the treatment, and cells treated with dual drug-loaded SWNHs were completely ablated, even where cells were cultured in normal media. The therapeutic effect of DOX and cisplatin was more clearly observed by the histological examination of treated cells. As shown in

Figure 4C, after the treated cells were maintained for 24 h, DOX (red florescence) was released from the system and cisplatin interacted with DNA, inducing cellular DNA damage (green florescence). For the dual drug-loaded SWNHs, the fluorescence signals from both DOX and cisplatin overlapped with that of DAPI (nuclear stain), indicating the simultaneous interaction of DOX and cisplatin with cellular DNA. Twenty-four hours after incubation, nuclei had shrunk considerably and few cells were observed in the culture dishes (Figure 4C, lower row).

Thermotherapy Potential Assay

To evaluate the potential of SWNHs for cell PTT, 4T1 cells were treated with 10 μg/mL of drug-free SWNHs and irradiated with an 808 nm laser at 0.4 W/cm² for different time intervals (3, 5 and 10 min). The treated cells were stained with calcein AM and propidium iodide (PI) to indicate the live and dead cells. As shown in Figure 5, cell death was negligible after 3 min irradiation and apparent after exposure for 5 min. Virtually no live cells were observed in the exposure area after laser irradiation for 10 min. These findings indicated that SWNHs had a strong thermal therapeutic effect on cancer cells and had potential for PTT in cancer.

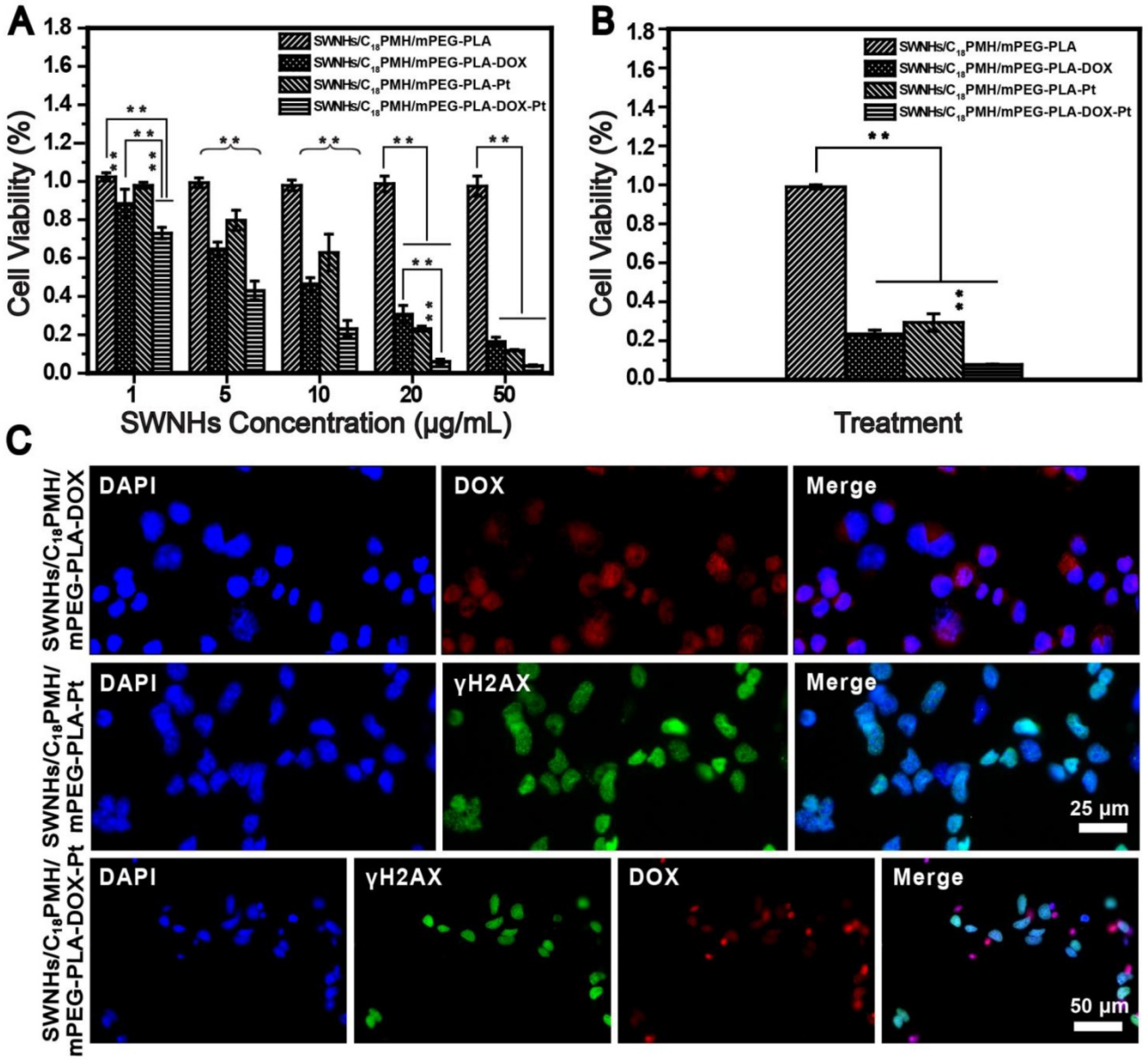

Figure 4. Synergetic chemotherapy with SWNHs/C_{18}PMH/mPEG-PLA-DOX in 4T1 cells. A) Viability of 4T1 cells after treatment with drug-free or drug-loaded SWNHs at different dosages (1, 5, 10, 20, and 50 μg SWNHs/mL) for 24 h. B) Viability of treated cells maintained in fresh culture medium for another 24 h. C) Fluorescence images of treated cells following maintenance in fresh culture medium for 24 h. ** $p < 0.01$.

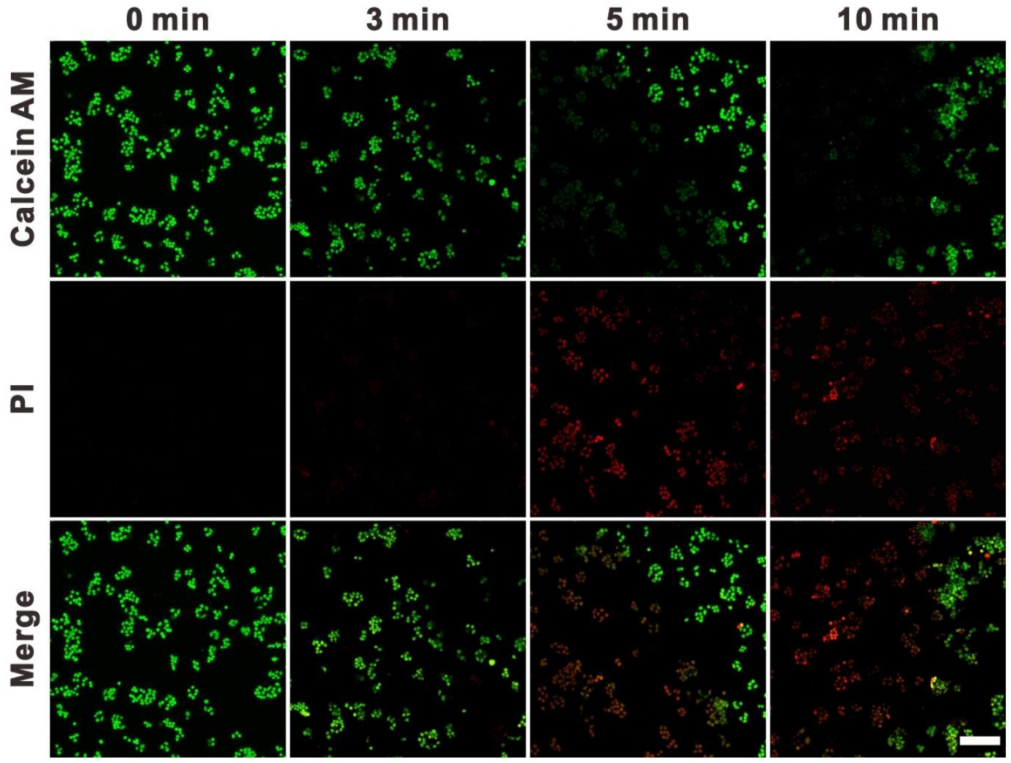

Figure 5. Fluorescence images of 4T1 cells co-stained with calcein AM (green) and PI (red). Cells were incubated with SWNHs/C_{18}PMH/mPEG-PLA (10 μg SWNHs/mL) for 24 h and irradiated with an 808 nm NIR laser at 0.4 W/cm² for various time intervals. Scale bar is 100 μm.

Chemo-Photothermal Combination Therapy *In Vitro*

Motivated by the highly effective cocktail chemotherapy and single PTT findings, we evaluated the potential of chemo-photothermal synergetic therapy of SWNHs/C_{18}PMH/mPEG-PLA-DOX-Pt on tumor cells. 4T1 cells treated with different doses of dual drug-loaded SWNHs for 24 h and illuminated with an 808 laser for 3 min at 0.4 W/cm² (72 J/cm²).

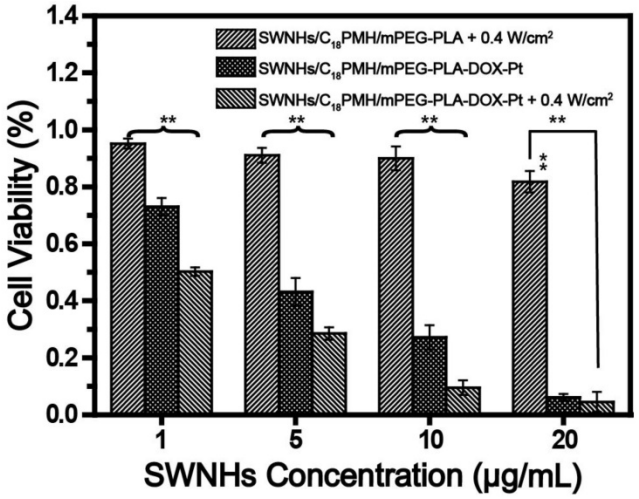

Figure 6. Chemo-photothermal combination therapy in 4T1 cells. For photothermal treatment, an 808 nm laser was used and the irradiation was conducted at a power density of 0.4 W/cm² for 3 min. After treatment, cells were further maintained for 24 h and cell viability was evaluated by CCK-8 assay. ** $p < 0.01$.

After treatment, cells were further maintained for 24 h, and cell viability was evaluated by CCK-8 assay. Photothermal treatment of cells incubated with drug-free SWNHs had a marginal effect on cell viability at concentrations below 10 μg/mL (Figure 6). However, the viability of cells incubated with dual drug-loaded SWNHs was 73.0% ± 2.9% at a dose of 1 μg/mL, and was significantly reduced after chemo-thermal combination therapy (50.3% ± 1.5%, $p < 0.01$). This phenomenon was also observed at doses of 5 and 10 μg/mL. The CI of chemo-photothermal combination therapy was determined to be 0.396. (Figure S5). In line with previous reports, these observations indicated that chemo-photothermal combination therapy has a synergetic therapeutic effect in cancer treatment [22, 23], which may result from the fact that the temperature rise, though insufficient to kill tumor cells, can increase cellular sensitivity to chemotherapeutic drugs, thus leading to enhanced antitumor effects [56].

It is worth noting that, compared with previous reports on chemo-thermal therapy that frequently apply high drug doses or relatively high laser powers [57-59], chemo-photothermal therapy with our dual drug-loaded SWNHs at a dose of 1 μg/mL in combination with 0.4 W/cm² laser exposure was sufficient for tumor cell killing. Lower doses and laser power densities are beneficial in cancer treatment, as

they not only reduce the systemic toxic effects of chemotherapy but also avoid skin burning or normal tissue damage by laser irradiation. These results supported the higher cytotoxic efficiency of the combined therapy than that of PTT or chemotherapy alone.

In Vivo Chemo-Photothermal Combination Therapy

Photoacoustic Imaging

Tumor accumulation is a major limitation of chemotherapeutic drug delivery in the treatment of solid tumors [5, 46]. To identify the accumulation of dual drug-loaded SWNHs in tumors and optimize the incubation time for thermal therapy, photoacoustic imaging of tumors was initially performed in five mice intravenously injected with SWNHs/C_{18}PMH/mPEG-PLA-DOX-Pt at a dose of 10 mg/kg body weight (b.w., in SWNHs). As shown in Figure 7A, PAI revealed that tumor accumulation of SWNHs/C_{18}PMH/mPEG-PLA-DOX-Pt increased with increased circulation time. Twenty-four hours after injection, tumor accumulation of nanohorns was pronounced. Nanohorns were mainly observed in tumor vessels initially, and then gradually permeated into the tumor parenchyma (Figure 7A, S6). Consistent with PAI observations, the corresponding PA signal intensity in tumor regions also increased steadily (Figure S6). Upon visual inspection, the tumor sites also appeared dark at 24 h post-injection (Figure 7B).

To corroborate the observations of PAI histologically and evaluate the possible chemotherapeutic effects of the loaded drugs at an early time point, mice were sacrificed after PAI. Tumors were harvested and tumor tissues were examined microscopically, indicating that nanohorns were deposited in the tumors and DOX was released from the SWNH carrier. Immunohistological staining against γH2AX indicated that cisplatin had induced dsDNA breakage (Figure 7C).

Chemo-Photothermal Combination Therapy

Next, we examined the potential of SWNHs/C_{18}PMH/mPEG-PLA-DOX-Pt for chemo-photothermal combination therapy of tumors *in vivo.* For this purpose, we first optimized the laser power intensity used for thermal therapy *in vivo*. Mice bearing 4T1 tumors were intravenously injected with dual drug-loaded SWNHs at a dosage of 10 mg/kg b.w. (in SWNHs), and 24 h post-injection, laser irradiation was performed at different power densities for different periods of time. The temperature at the tumor sites was monitored with an IR thermal camera. As shown in Figures S7 and S8, temperature elevation was mainly laser power dependent and rapidly rose to ~60 °C after irradiation at 1 W/cm^2 for 5 min (300 J/cm^2). It has been reported that temperatures above 50 °C are sufficiently high for tumor ablation [22, 23, 50]. Therefore, the laser power intensity of 1 W/cm^2 and irradiation for 5 min was

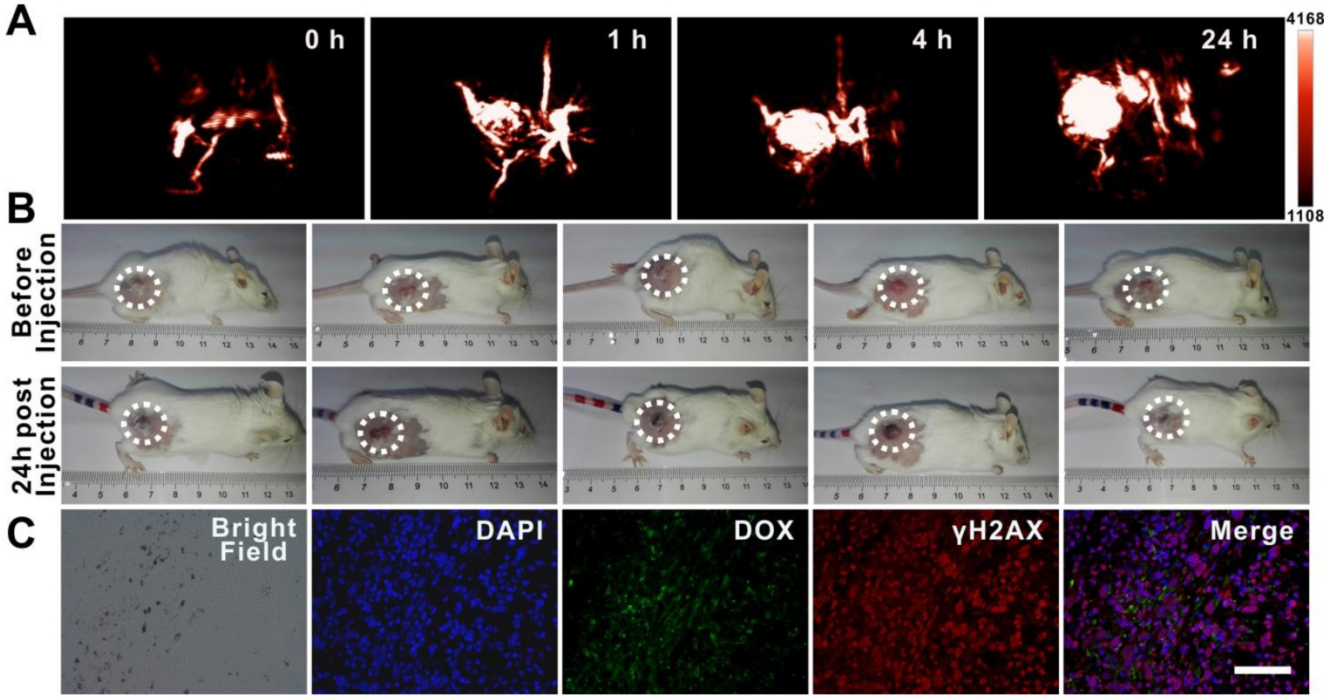

Figure 7. Tumor accumulation of dual drug-loaded SWNHs. A, B) Photoacoustic imaging of tumors at different time intervals after mice were intravenously injected with SWNHs/C_{18}PMH/mPEG-PLA-DOX-Pt (10 mg SWNHs/kg body weight) and photographs of tumors 24 h post-injection. C) Histological studies of tumor tissues 24 h post-injection. Scale bar is 100 μm.

used as an optimum condition for the subsequent thermal treatment of tumors.

For chemo-photothermal combination therapy, mice bearing 4T1 tumors (~300 mm^3 in volume) were divided into five groups with 13 mice in each group: (1) PBS + laser, (2) SWNHs/C_{18}PMH/mPEG-PLA, (3) SWNHs/C_{18}PMH/mPEG-PLA-DOX-Pt, (4) SWNHs/C_{18}PMH/mPEG-PLA + laser, and (5) SWNHs/C_{18}PMH/mPEG-PLA-DOX-Pt + laser. The drug-free and drug-loaded SWNHs were intravenously injected at a dosage of 10 mg/kg b.w. (in SWNHs) only once, corresponding to 4.4 mg DOX/kg b.w. and 6.6 mg cisplatin/kg b.w., doses that were lower than those used in clinical applications [6, 7, 60].

As shown in Figure 8A, following irradiation at the optimized conditions, the temperature at the tumor sites of mice treated with SWNHs/C_{18}PMH/mPEG-PLA-DOX-Pt and SWNHs/C_{18}PMH/mPEG-PLA elevated rapidly and reached 60.9 °C and 61.6 °C, respectively. For the mice receiving PBS, however, temperature elevation was unnoticeable. After thermal treatment, three mice from each group were sacrificed, tumors were harvested, and tumor tissues were stained by hematoxylin and eosin (H&E) to examine the therapeutic effect immediately after treatment. The tumor cells grew densely in the PBS + laser, SWNHs/C_{18}PMH/mPEG-PLA-DOX-Pt, and SWNHs/C_{18}PMH/mPEG-PLA treatment groups, while in the SWNHs/C_{18}PMH/mPEG-PLA-DOX-Pt + laser and SWNHs/C_{18}PMH/mPEG-PLA + laser treatment groups, they contracted severely and the tumors became loose and fragile (Figure 8B). These results, consistent with previous reports [22], indicated that thermal therapy with SWNHs/C_{18}PMH/mPEG-PLA-DOX-Pt could damage tumors immediately after treatment.

Following treatment, the remaining mice were followed for up to 65 days, during which time tumor sizes were measured and mouse survival recorded. Compared with the PBS + laser and SWNHs/C_{18}PMH/mPEG-PLA groups, which exhibited approximately 13.5- and 12.5-fold increases in tumor volume, tumor growth in the SWNHs/C_{18}PMH/mPEG-PLA-DOX-Pt treatment group was significantly suppressed, with an approximately 6.3-fold increase in tumor volume ($p < 0.01$, Figure 8C). However, for the SWNHs/C_{18}PMH/mPEG-PLA + laser and SWNHs/C_{18}PMH/mPEG-PLA-DOX-Pt + laser treatment groups, the tumors began to shrink immediately after laser exposure and were completely ablated by 16 days after treatment. However, single thermal treatment (SWNHs/C_{18}PMH/mPEG-PLA + laser) did not prolong the survival of mice, similar to the PBS + laser and SWNHs/C_{18}PMH/mPEG-PLA treatment groups. In contrast, dual drug chemotherapy (SWNHs/C_{18}PMH/mPEG-PLA-DOX-Pt) and chemo-photothermal combination therapy (SWNHs/C_{18}PMH/mPEG-PLA-DOX-Pt + laser) significantly extended the life span of mice. For chemo-photothermal combination therapy in particular, all mice had survived by 65 days after treatment (Figure 8D).

Pharmacokinetics, Biodistribution, and *Ex Vivo* DOX Fluorescence Imaging

4T1 cell is a murine breast cancer cell line with a high rate of recurrence and metastasis, particularly to the lung [51, 52, 61]. To investigate whether mouse death was related to tumor metastasis, we examined the lungs histologically using H&E staining before treatment and with India ink staining after treatment for mice who had died during the maintenance period. Consistent with previous findings [62-64], all mice were found to have developed lung metastases two week after tumor implantation (Figure 8E). Treatment with PBS + laser or SWNHs/C_{18}PMH/mPEG-PLA did not ablate the metastatic nodules or inhibit further tumor metastasis (Figure 9A). Although the primary tumors were completely eradicated at 16 days post-thermal treatment in the SWNHs/C_{18}PMH/mPEG-PLA + laser group, 80% of mice suffered tumor recurrence or lung metastasis. Combination chemotherapy with SWNHs/C_{18}PMH/mPEG-PLA-DOX-Pt largely ablated or inhibited tumor metastasis, and only 40% of mice in this group developed lung metastases. However, tumor metastatic nodules or recurrence was not found in the SWNHs/C_{18}PMH/mPEG-PLA-DOX-Pt + laser treatment group. Chemo-photothermal combination therapy with SWNHs/C_{18}PMH/mPEG-PLA-DOX-Pt not only eliminated the primary tumors and metastatic nodules that already existed prior to treatment but also suppressed tumor recurrence *in situ* and further metastasis to the lung. Recently, it has been reported that photothermal treatment of tumors could largely evoke host immunity and induce the abscopal effect and long-term immune-memory effect, leading to inhibition of tumor growth at distant sites and prevention of tumor recurrence [20, 21, 63]. Therefore, we speculated that in addition to dual-drug chemotherapy, the immune response induced by thermal treatment of the primary tumors might partially contribute to the elimination of their lung metastases. However, further efforts are warranted to understand the mechanisms.

To provide a further insight into why SWNHs/C_{18}PMH/mPEG-PLA-DOX-Pt + laser had a superior therapeutic efficacy, the blood half-life and biodistribution of the nanohorns were evaluated. For both studies, six mice were intravenously

administered SWNHs/C_{18}PMH/mPEG-PLA-DOX-Pt at a dosage of 10 mg/kg b.w. (in SWNHs) and blood samples were collected from the tail veins of three mice at different time points. The half-life of SWNHs/C_{18}PMH/mPEG-PLA-DOX-Pt by PA signal intensity was fitted to a two-compartment bolus intravenous injection model and determined using bi-exponential nonlinear regression [65, 66]. As shown in Figure 9B, the elimination half-life of dual drug-loaded SWNHs was 10.9 h. A prolonged blood circulation time has been shown to be beneficial for tumor accumulation of nanohorns through the EPR effect [32, 33, 67].

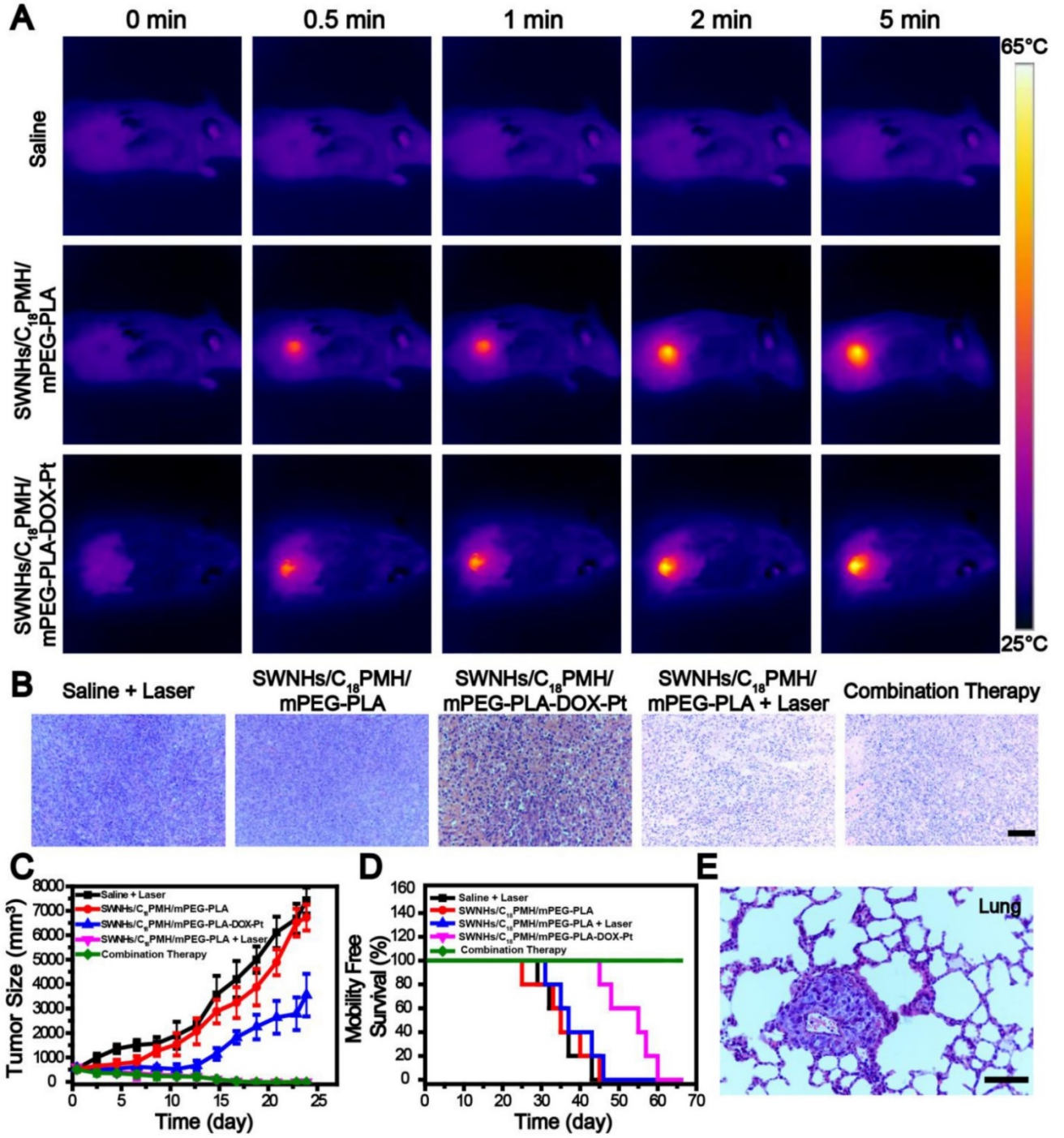

Figure 8. Chemo-photothermal combination therapy in tumors. A) Infrared thermographic maps of tumors exposed to an 808 nm laser at 1 W/cm² 24 h after tumor-bearing mice were intravenously injected with PBS, SWNHs/C_{18}PMH/mPEG-PLA, or SWNHs/C_{18}PMH/mPEG-PLA-DOX-Pt (10 mg SWNHs/kg body weight). B) H&E staining of tumor tissues immediately after laser treatment. Scale bar: 100 μm. C) Relative tumor size and D) survival of mice in different treatment groups. E) H&E staining of lung tissues before treatment. Mice had already developed lung metastases prior to treatment. Scale bar is 100 μm.

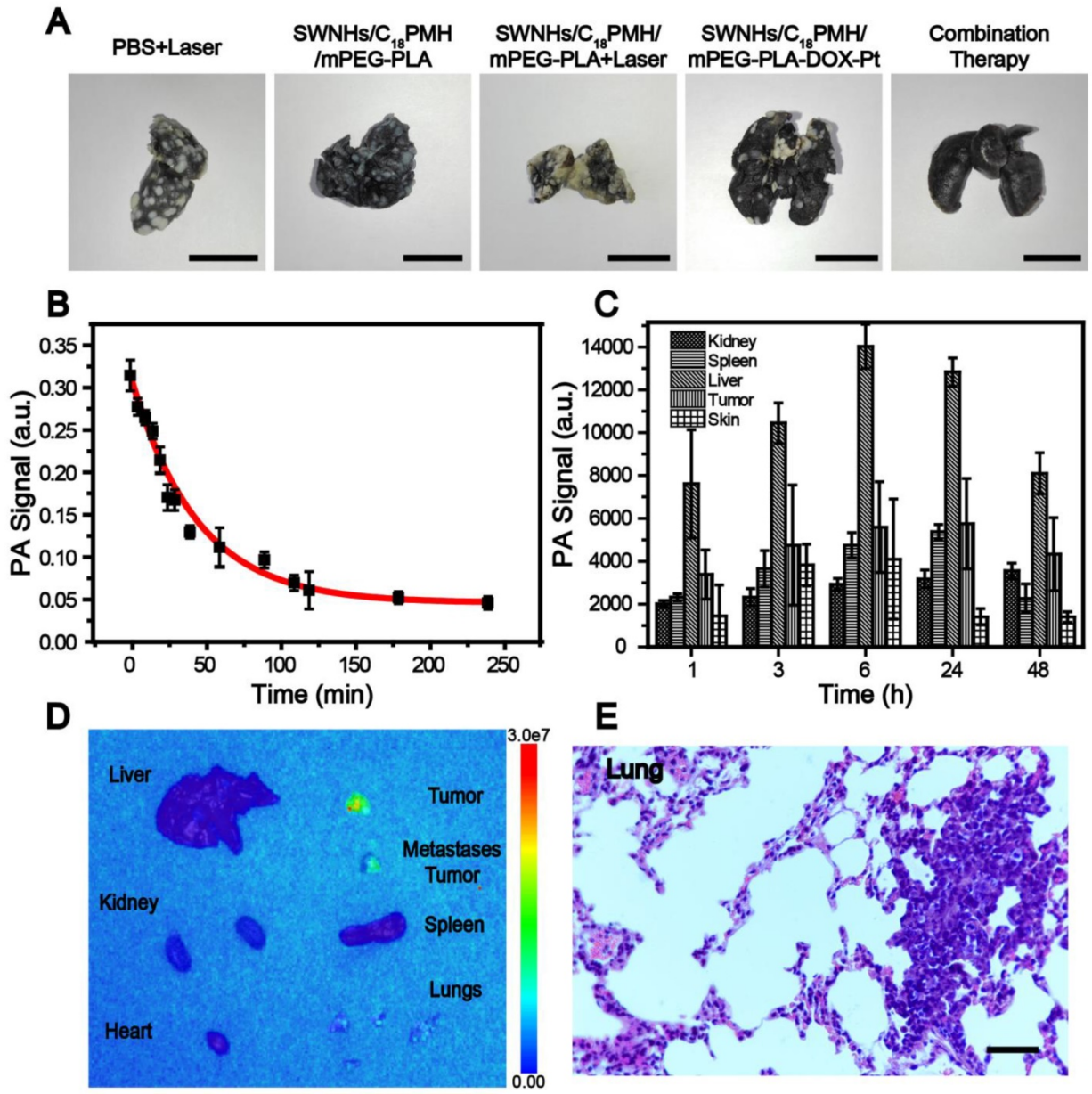

Figure 9. A) India ink staining of lungs from different treatment groups. Scale bar is 1 cm. B) Blood circulation time and C) bio-distribution of SWNHs/C_{18}PMH/mPEG-PLA-DOX-Pt evaluated by PAI. D) *Ex vivo* fluorescence images of major organs and tumors 24 h post injection of SWNHs/C_{18}PMH/mPEG-PLA-DOX-Pt. E) H&E staining of lung tissues after fluorescence imaging. The metastatic nodules can be clearly observed. Scale bar is 100 μm.

The bio-distribution of SWNHs in the major organs was studied *in vivo* using PAI and their accumulation in tumors was further examined *ex vivo* by fluorescence imaging at 24 h post-injection. For PAI, organs were first localized by ultrasound imaging before PAI was conducted and the signal intensities in each organ were measured. As shown in Figure 9C, SWNHs were mainly sequestered by the liver, similar to other nanoformulations [34, 68, 69], and moderately accumulated in tumors.

As demonstrated previously, an acid environment is favorable for DOX release from SWNHs and, once released, its fluorescence can be recovered. Therefore, after the bio-distribution study, the mice were sacrificed, major organs were removed, and *ex vivo* fluorescence imaging was conducted. As shown in Figure 9D, strong fluorescence was observed in both primary tumors and larger metastatic nodules excised from the lung. Even in smaller metastatic nodules, fluorescence signal was also discernible. The presence of metastatic nodules was verified by H&E staining of lung tissues after *ex vivo* fluorescence imaging (Figure 9E). However, no fluorescence signal was detected in other organs, despite the obvious accumulation of drug-loaded SWNHs as shown in the bio-distribution study. These phenomena may be ascribed to the marginal release of DOX observed under physiological conditions (pH

7.4). Our findings indicated that in addition to targeting the initial tumors, SWNHs/C_{18}PMH/mPEG-PLA-DOX-Pt were capable of simultaneously targeting lung metastatic nodules with high efficiency, a characteristic that may be attributable to its long blood half-life, unique structure, and favorable size for tumor targeting through the EPR effect [32, 33, 66].

Finally, we examined the potential toxic effects of the dual drug-loaded SWNHs. Major organs (heart, liver, spleen, lung, and kidney) from each treatment group were obtained from sacrificed mice. For the SWNHs/C_{18}PMH/mPEG-PLA-DOX-Pt + laser group, mice were sacrificed 65 days after treatment. Histological analyses revealed no noticeable organ damage or significant abnormalities except for the metastatic nodules observed in the lungs of animals in the PBS + laser, SWNHs/C_{18}PMH/mPEG-PLA, SWNHs/C_{18}PMH/mPEG-PLA-DOX-Pt, and SWNHs/C_{18}PMH/mPEG-PLA + laser treatment groups (Figure 10). These preliminary results indicated that SWNHs/C_{18}PMH/mPEG-PLA-DOX-Pt exhibited no obvious short-term toxicity in mice at the dose used in the present study.

Conclusion

In summary, we have developed a robust, dual drug-loaded, chemo-photothermal theranostic system based on SWNHs, termed SWNHs/C_{18}PMH/mPEG-PLA-DOX-Pt, for PAI-guided tumor therapy. By rationally engineering the surface of SWNHs with C_{18}PMH and mPEG-PLA, DOX and cisplatin could be sequentially loaded onto the nanohorns with high efficiency and lack of interference and released in a pH-responsive, tandem, and sustainable manner. More significantly, SWNHs/C_{18}PMH/mPEG-PLA-DOX-Pt demonstrated both dual drug chemotherapeutic and chemo-photothermal synergetic anti-tumor effects. As a result, tumor cells were completely ablated by chemo-photothermal therapy using relatively mild conditions. For solid tumor treatment, dual drug-loaded SWNHs exhibited prolonged blood circulation and could simultaneously and efficiently target both the primary tumors and their lung metastases. Consequently, chemo-photothermal treatment of primary tumors guided by PAI eradicated the primary and metastatic tumors. Our study demonstrates the considerable potential of SWNHs/C_{18}PMH/mPEG-PLA-DOX-Pt for tumor chemo-photothermal combination therapy.

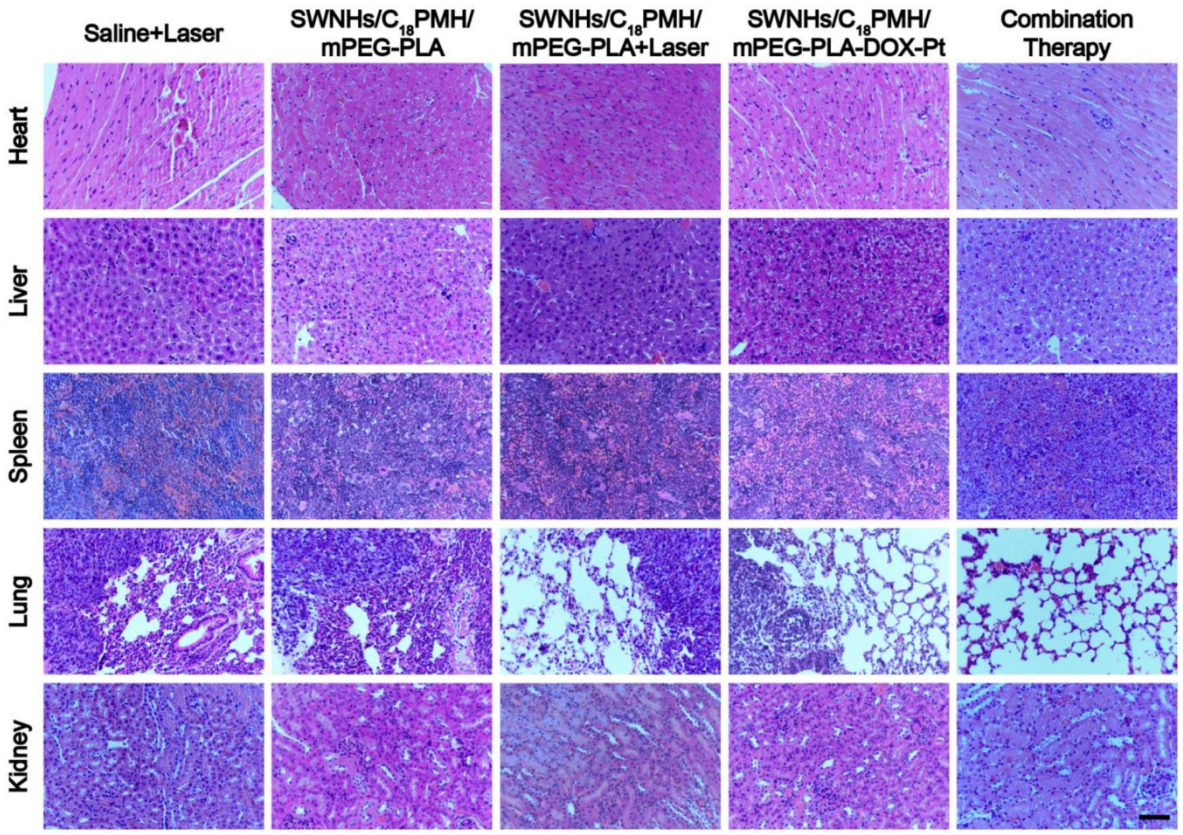

Figure 10. H&E staining of major organs from mice in different treatment groups. Scale bar is 100 μm.

Materials and Methods

Synthesis and Characterization of SWNHs/C_{18}PMH/mPEG-PLA-DOX-Pt

Modification of single-walled nanohorns (SWNHs): SWNHs were purchased from NEC Company (Tokyo, Japan) and modified simultaneously with maleic anhydride-alt-1-octadecene (C_{18}PMH, MW 1051 Da) and methoxypolyethyleneglycol-b-poly-D, L-lactide (mPEG-PLA, MW 5K–5K Da). Specifically, C_{18}PMH (5 mg) and mPEG-PLA (5 mg) were dissolved in 200 μL of tetrahydrofuran, into which 4 mL of deionized water was then added. The mixture was stirred for 1 h at room temperature under nitrogen gas to evaporate the tetrahydrofuran. Subsequently, SWNHs (1 mg) were suspended into the mixture and sonicated for 1 h at room temperature to yield a black suspension. The suspension was centrifuged at 12,857 ×g for 30 min to remove any large SWNH aggregates. The modified SWNHs, termed SWNHs/C_{18}PMH/mPEG-PLA, were retrieved by ultrafiltration (Millipore, MWCO 100 K) and freeze-dried.

DOX loading: SWNHs/C_{18}PMH/mPEG-PLA (0.5 mg) were suspended in 1 mL of DOX aqueous solution at different concentrations (0.5, 1, 1.5, and 2 mg/mL) and sonicated for 1 h. Next, the product was transferred to a dialysis bag (MWCO, 14 KDa) and dialyzed against deionized water overnight at room temperature to remove free DOX. The drug-loading capacity (DLC) and drug-loading efficiency (DLE) were evaluated spectrofluorometrically against known standards at an excitation wavelength of 480 nm and emission of 593 nm, and were determined according to the following equations [9, 14]:

$$\text{DLC}\ (\%) = \frac{\text{initial wt of drug -wt of drug in supernatant}}{\text{wt of drug loaded nano vehicles}} \times 100\% \quad (1)$$

$$\text{DLE}\ (\%) = \frac{\text{wt of drug in nano vehicles}}{\text{wt of drug in feed}} \times 100\% \quad (2)$$

DOX-loaded SWNHs/C_{18}PMH/mPEG-PLA, designated as SWNHs/C_{18}PMH/mPEG-PLA-DOX, were freeze-dried for further use.

Cisplatin loading: Cisplatin loading was performed according to previous reports [22, 43, 44]. First, cisplatin $[Pt(H_2O)_2(NH_3)_2](Cl)_2$ was activated by silver nitrate to form $[(NH_2)_2Pt(H_2O)_2](NO_3)_2$. Subsequently, various amounts of $[Pt\ (H_2O)_2(NH_3)_2]^{2+}$ were added into the SWNHs/C_{18}PMH/mPEG-PLA-DOX suspension (1 mL, in tris-tricine buffer, pH = 8.3) and gently mixed for 1 h at room temperature. Free cisplatin was removed by dialysis (MWCO, 3 kDa) against PBS (pH = 7.4) overnight and quantified by inductively coupled plasma mass spectroscopy (ICP-MS, iCAP-Q, Thermo Scientific, USA). Accordingly, DLC and DLE were calculated. Moreover, the release of DOX during cisplatin loading and the subsequent dialysis was also measured and the contents of DOX and cisplatin in the final formulation were then determined. The dual drug-loaded SWNHs, SWNHs/C_{18}PMH/mPEG-PLA-DOX-Pt, were freeze-dried.

Single drug-loaded SWNHs, SWNHs/C_{18}PMH/mPEG-PLA-DOX and SWNHs/C_{18}PMH/mPEG-PLA-Pt, with the same DLC and DLE as those of the dual drug-loaded SWNHs, were also prepared according to the same procedure.

Characterization: The sizes and zeta potentials of the drug-free, single drug-, and dual drug-loaded SWNHs were characterized by dynamic light scattering (DLS, Malvern Zetasizer Nano ZSP, Malvern, United Kingdom) in deionized water at 25°C. Transmission electron microscopy (TEM) images were obtained from JEM-2011 (JEOL, Japan) at 200 kV. NIR absorption spectra were recorded with a NanoDrop 1000 (Thermo Scientific, Wilmington, USA) and UV/Vis/NIR spectrophotometer (F-2700, HITACHI, Tokyo, Japan).

Drug release *in vitro*

To determine the release profiles of DOX and cisplatin, lyophilized SWNHs/C_{18}PMH/mPEG-PLA-DOX-Pt (1 mg) was suspended in 1 mL of PBS (10 mM) at different pH values (3.8, 5.5, 7.4, and 9.0). The suspensions were transferred into dialysis tubing (MWCO, 1 KDa), soaked in 20 mL of PBS (10 mM) in glass vials, and maintained in a horizontal shaker at 37°C and 120 rpm. Next, 100 μL of dialysate from each sample was displaced with 100 μL of fresh PBS at the predefined time intervals. The amounts of DOX and cisplatin released from the SWNHs/C_{18}PMH/mPEG-PLA-DOX-Pt were measured using a UV-vis spectrophotometer (Thermo Scientific, USA) by absorbance at 480 nm and by ICP-MS, respectively.

The cumulative release of drug was calculated as described previously:

$$\text{Cumulative release}\ \% = \frac{\left(C_n \times V + V_i \sum_{i=0}^{n-1} Ci\right)}{\left(m_{\text{drug loaded}}\right)} \times 100\% \quad (3)$$

Where C_n is the concentration of drug in the filtrate solution and V is the volume of supernatant taken each time (100 μL). $m_{drug\ loaded}$ represents the mass of drug loaded onto the SWNHs.

Photothermal performance of the dual drug-loaded SWHNs

To assess the photothermal performance of the dual drug-loaded SWNHs, lyophilized SWNHs/C_{18}PMH/mPEG-PLA-DOX-Pt were suspended into 400 μL of PBS at different concentrations (10, 30, 50,

and 100 μg/mL in SWNHs) and illuminated with an 808 nm laser at a power intensity of 1 W/cm², or at a concentration of 50 μg/mL and a series of power densities (0, 0.5, 1, and 2 W/cm²). A digital thermometer was used to monitor temperature change with a thermocouple probe submerged in the solution. To test the thermal stability of the probe, SWNHs/C_{18}PMH/mPEG-PLA-DOX-Pt (50 μg/mL) were irradiated six times with a power density of 1 W/cm² for 5 min (300 J/cm²). The distance between laser lens and samples was set to 20 cm. The spot diameter was 0.5 cm. The laser power density was calibrated by photo radiometer PL-MW 2000 (Perfectlight CO., LTD., Beijing, China). These parameters were also used for the following *in vitro* experiments that involved photothermal therapy.

Synergetic Chemotherapy with SWNHs/C_{18}PMH/mPEG-PLA-DOX-Pt

Cell culture: 4T1 cells, a murine breast cancer cell line, were cultured in Roswell Park Memorial Institute-1640 (RPMI-1640) medium with 10% FBS, 100 IU/mL penicillin, and 100 mg/mL streptomycin sulfate (PS) at 37 °C under a humidified atmosphere of 5% CO_2.

CCK-8 assay: 4T1 cells were seeded into 96-well culture plates (1×10^4 cells per well) and cultured with medium containing SWNHs/C_{18}PMH/mPEG-PLA, SWNHs/C_{18}PMH/mPEG-PLA-DOX, SWNHs/C_{18}PMH/mPEG-PLA-Pt, or SWNHs/C_{18}PMH/mPEG-PLA-DOX-Pt at a series of concentrations (1, 5, 10, 20, or 50 μg/mL in SWNHs) for 24 h. Next, cell viability was determined using a Cell Counting Kit-8 (CCK-8) assay according to the manufacturer's instructions [22]. Briefly, after treatment, the culture medium was removed and cells were replenished with 100 μL of fresh RPMI-1640 medium containing 10 μL of CCK-8 regent. After incubation for another 1 h, the absorbance of each well was measured at 450 nm with a plate reader (PerkinElmer, Baltimore, MD). Cell viability was expressed as a percentage of the absorbance of cells incubated with the SWNHs to that of cells maintained in normal culture medium.

Accordingly, the IC_{50} values (half-maximal inhibitory concentration) of SWNHs/C_{18}PMH/mPEG-PLA-DOX, SWNHs/C_{18}PMH/mPEG-PLA-Pt, or SWNHs/C_{18}PMH/mPEG-PLA-DOX-Pt were determined from dose-response curves. IC_{50} values of free DOX, cisplatin, and DOX/cisplatin combination were also evaluated. The combination index (CI), which indicates the type of anticancer mechanism of the combined drugs, was calculated according to the formula $CI = C_1/C_{x1} + C_2/C_{x2}$, where C_1 and C_2 are the concentrations of the first and the second drug required to achieve a certain effect in combination therapy, and C_{x1} and C_{x2} are the concentrations of the first and the second drugs that generate the identical effect alone. When CI > 1, = 1, or < 1, the two drugs are implied to have antagonistic, additive, or synergistic effects, respectively [9, 14, 70].

To further demonstrate the synergetic therapeutic effect of the two drugs, 4T1 cells were incubated with single drug-loaded or dual drug-loaded SWNHs at a dose of 10 μg/mL for 24 h. Subsequently, the culture media were removed and cells maintained in fresh media for another 24 h. Cell viability was examined by CCK-8 assay, as described above.

Histological studies of treated cells

To demonstrate the simultaneous therapeutic effect of DOX and cisplatin on tumor cells, 4T1 cells were seeded onto cover slips in 6-well plates and treated with SWNHs/C_{18}PMH/mPEG-PLA-DOX, SWNHs/C_{18}PMH/mPEG-PLA-Pt, or SWNHs/C_{18}PMH/mPEG-PLA-DOX-Pt at a dosage of 10 μg/mL for 24 h. After treatment, the cells were washed with PBS (pH 7.4) three times and maintained for 24 h in fresh culture medium. Next, cells were fixed with 4% paraformaldehyde. γH2AX is a biomarker of double-strand DNA breakage and is frequently used to evaluate the DNA damage induced by cisplatin [43, 71]. To examine the therapeutic effect of cisplatin, cells were immunostained for γH2AX as follows: Fixed cells were blocked with 10% goat serum in 0.5% Triton X-100 in PBS for 20 min. After three washes with PBS, cells were incubated with monoclonal antiphosphohistone γ-H2AX primary antibody (2 μg/mL; Millipore, Billerica, MA, USA) containing 1% bovine serum albumin (BSA) at 4 °C overnight. After washing with PBS (pH 7.4) three times, cells were further incubated with Alexa Fluor 488 goat anti-rabbit secondary antibody (1:300 dilution; Molecular Probes, Eugene, OR) for 1 h at room temperature. Cell nuclei were counterstained with DAPI. As DOX could recover its fluorescence following its release from SWNHs, the release of DOX in cells could be directly observed upon excitation at a wavelength of 480 nm. Cells were examined using a dark-field fluorescence microscope (Nikon ECLIPSE Ti-E, Tokyo, Japan).

Thermotherapy potential assay

To evaluate the potential of the SWNHs for cell photothermal therapy, 4T1 cells were seeded onto cover slips in 6-well plates and treated with 10 μg/mL of SWNHs/C_{18}PMH/mPEG-PLA for 24 h. Next, cells were washed with PBS three times, replenished with fresh culture medium, and illuminated with an 808 laser at 0.4 W/cm² for 3, 5, or 10 min. After treatment, calcein AM (2 μM) and propidium iodine (PI)

solutions (4 μM) were added to the cell culture media and incubated for 30 min. Finally, cells were washed with PBS three times and fluorescence imaging of cells was performed using a Nikon ECLIPSE Ti-E fluorescence microscope (Tokyo, Japan) with a 10× objective lens.

Chemo-photothermal combination therapy *in vitro*

To evaluate the potential chemo-photothermal synergetic therapy of SWNHs/C_{18}PMH/mPEG-PLA-DOX-Pt on tumor cells, 4T1 cells were seeded onto 96-well plates and treated with different concentrations of the dual drug-loaded SWNHs (1, 5, 10, and 20 μg/mL in SWNHs) for 24 h. After treatment, culture media were removed and cells were washed with PBS three times and supplemented with fresh media (RPMI-1640, 200 μL/well). Subsequently, photothermal treatment was conducted by illuminating the treated cells with an 808 nm laser at a power density of 0.4 W/cm^2 for 3 min (72 J/cm^2). After treatment, cells were further maintained for 24 h and cell viability was evaluated by CCK-8 assay, as described previously. The chemo-photothermal combination index was calculated according to the formula $CI = C_1/C_{x1} + C_2/C_{x2}$, where C_1 and C_2 are the concentration of SWNHs/C_{18}PMH/mPEG-PLA-DOX-Pt to achieve a certain effect in combination therapy, and C_{x1} and C_{x2} are the concentrations of SWNHs/C_{18}PMH/mPEG-PLA-DOX-Pt and the drug free SWNHs (SWNHs/C_{18}PMH/mPEG-PLA) that generate the identical effect alone [70, 72].

In Vivo Chemo-Photothermal Combination Therapy

Animal model

All animal experiments were performed in compliance with the National Regulations for the Administration of Affairs Concerning Experimental Animals and approved by the animal protection and care committee of Shanghai Jiao Tong University. Female balb/c mice were purchased from Slac Laboratory Animal Co. Ltd. (Shanghai, China) and housed under standard conditions at 20 ± 2 °C and 60% ± 10% relative humidity with a 12 h light/dark cycle. When the mice reached about 20 g in weight, tumor xenografts were generated by the subcutaneous injection of 4T1 cells (2×10^5) into the right flank of mice. Tumor size was measured using calipers and the volume was calculated according to the following equation [22]:

$$\text{Tumor volume (mm}^3\text{)} = \text{width}^2 \times \frac{\text{length}}{2} \quad (4)$$

When tumor volumes reached ~300 mm^3 (approximately 2 weeks after tumor implantation), the following experiments were carried out.

Photoacoustic imaging

To evaluate the tumor accumulation of SWNHs/C_{18}PMH/mPEG-PLA-DOX-Pt and optimize the time point for thermal treatment of tumors, photoacoustic imaging (PAI) of tumors was conducted using the Nexus128 (Endra Co. Ltd., MI, USA) and Vevo 3100 (Visualsonics, Fujifilm, Tokyo, Japan) PAI systems. Six mice, three for each PAI system, were intravenously injected with SWNHs/C_{18}PMH/mPEG-PLA-DOX-Pt at a dose of 10 mg/kg b.w. (in SWNHs). After injection, mice were scanned at different time intervals (0, 1, 4, and 24 h). The data were collected and analyzed by software provided by the manufacturers to reconstruct the tumor images. Photoacoustic signals of oxy/deoxy-hemoglobin and tissue before injection were used as controls.

After imaging, the mice were euthanized and tumors were harvested to histologically examine the accumulation of dual drug-loaded SWNHs. Tumors were fixed with paraformaldehyde (4%), imbedded in paraffin, and sliced into 6 μm thick sections. The sections were dewaxed in xylene and dehydrated in ethanol. Some slices were examined under bright-field microscopy. To determine whether cisplatin exerted a therapeutic effect, some tumor slices were stained for γH2AX using the same procedure as that described above for cell staining.

Chemo-photothermal combination therapy

Before performing photothermal therapy, the laser power intensity used for the therapy was optimized *in vivo*. Three 4T1 tumor-bearing mice were intravenously injected with SWNHs/C_{18}PMH/mPEG-PLA-DOX-Pt at a dose of 10 mg/kg b.w. (in SWNHs), and 24 h post-injection, an 808 nm laser was used to expose the tumors to a series of power densities (0, 0.5, 1, and 2 W/cm^2) for different periods of time. The distance between laser lens and tumors was set to 20 cm and the laser spot diameter was 1 cm. The temperature at the tumor sites was monitored using an IR thermal camera (S6, IRS Co. Ltd., Shanghai, China).

For chemo-phototherapy, 4T1 tumor-bearing mice were divided into five groups with 13 mice in each group: (1) PBS + laser, (2) SWNHs/C_{18}PMH/mPEG-PLA, (3) SWNHs/C_{18}PMH/mPEG-PLA-DOX-Pt, (4) SWNHs/C_{18}PMH/mPEG-PLA + laser, and (5) SWNHs/C_{18}PMH/mPEG-PLA-DOX-Pt + laser. Both the drug-free and drug-loaded SWNHs were intravenously injected *via* the tail vein at a dose of 10 mg/kg b.w. (in SWNHs, corresponding to 4.4 mg

DOX/kg b.w. and 6.6 mg cisplatin/kg b.w. for drug-loaded ones). Twenty-four hours post-injection, the tumors were irradiated with an 808 nm laser at a power density of 1 W/cm² for 5 min (300 J/cm²). An IR thermal camera (IRS System Inc., Shanghai, China) was used to record the temperature change in the tumor region. After treatment, tumor growth and mouse survival were monitored.

Pharmacokinetics, bio-distribution, and *ex vivo* DOX fluorescence imaging

Three 4T1 tumor-bearing mice were intravenously injected with SWNHs/C_{18}PMH/mPEG-PLA-DOX-Pt at a dose of 10 mg/kg b.w. (in SWNHs). To determine the blood half-life of the probe, blood samples (20 μL) were collected from the tail vein at different time points after injection and placed in plastic capillary tubes. PAI was performed using the Vevo 3100 system (Visualsonics Fujifilm, Tokyo, Japan) and the signal intensity of each sample was analyzed. The signal intensity half-life of SWNHs/C_{18}PMH/mPEG-PLA-DOX-Pt was fitted to a two-compartment bolus intravenous injection model [65] and determined using bi-exponential nonlinear regression with graphing software (GraphPad Prism 7.0) [65, 66].

For the bio-distribution study, three tumor-bearing mice were intravenously injected with SWNHs/C_{18}PMH/mPEG-PLA-DOX-Pt at a dose of 10 mg SWNHs/kg b.w. Twenty-four hours after injection, PAI was carried out in tumors and major organs (liver, spleen, lung, kidney, and skin) using a VevoLAZR 3100 system. The organs were located with an ultrasound imaging device integrated to the system and the signal intensity of each organ, representing the relative distribution of the probe, was recorded [73, 74].

For *ex vivo* fluorescence imaging, the mice were sacrificed after the bio-distribution study. Tumors and major organs (heart, liver, spleen, lung, and kidney) were removed and fluorescence imaging were conducted using an Amiview X imaging system (Spectral Instruments Imaging Co. Ltd., Tucson, AZ, USA) at the excitation wavelength of DOX (480 nm).

India ink staining of lung

To identify potential lung metastases, five mice were randomly selected and sacrificed immediately after the injection of India ink (15%) into the lungs through the trachea [61]. Subsequently, the lungs were collected, soaked in Fekete's solution (50 mL of 70% alcohol, 5 mL of formalin, and 2.5 mL of glacial acetic acid) at room temperature for 2–3 days, and photographed. White spots on black-stained lungs were determined as tumor metastasis sites.

Histological examination

Major organs (heart, liver, spleen, lung, and kidney) from each treatment group were harvested when mice died or after mice were sacrificed (SWNHs/C_{18}PMH/mPEG-PLA-DOX-Pt + laser group). For histological examination, the organs were fixed in 4% formalin, imbedded in paraffin, and processed for hematoxylin and eosin (H&E) (Aladdin, Ontario, CA, USA) staining according to the protocol provided by the manufacturer and previous reports [75]. Tissue slices were examined under a digital microscope (Nikon ECLIPSE Ti-E, Tokyo, Japan).

Statistical evaluation

Data from each experiment are expressed as mean ± standard deviation (n = 3). Statistical analysis was conducted using Student's *t* test. A p value of <0.05 was considered to indicate significant differences between groups.

Abbreviations

SWNHs: single-walled carbon nanohorns; DOX: doxorubicin; PAI: photoacoustic imaging; AML: acute myelocytic leukemia; PTT: photothermal therapy; EPR: enhanced permeability and retention; DLC: drug-loading capacity; DLE: drug-loading efficiency; TEM: transmission electron microscopy; FBS: fetal bovine serum; PBS: phosphate buffer solution; RPMI-1640: Roswell Park Memorial Institute-1640; CCK-8: Cell Counting Kit-8; IC_{50}: half-maximal inhibitory concentration; CI: combination index; PI: propidium iodide; H&E: Hematoxylin and Eosin.

Supplementary Material

Supplementary figures for characterization of the SWNHs; stability of the nanoformulation in the physiological environment; UV–VIS-NIR spectra and fluorescence images before and after DOX loaded on nano vehicle; evaluation of half-maximal inhibitory concentration of various nanoformulation; photoacustic imaging and infrared thermographic maps of 4T1 tumor-bearing mice; change of temperature on tumor site during laser irradiation (Fig. S1-S8); Table S1: Zeta potentials of the drug-free and drug-loaded SWNHs; Table S2: Drugs loading on the modified SWNHs.
Supplementary figures and tables.
http://www.thno.org/v08p1966s1.pdf

Acknowledgements

This work was supported by the National Natural Science Foundation of China (grant 81571729, 81230030) and the Med-Engineering Crossing Foundation from Shanghai Jiao Tong University (YG2017ZD05).

Competing Interests

The authors have declared that no competing interest exists.

References

1. Woodcock J, Griffin JP, Behrman RE. Development of Novel Combination Therapies. N Engl J Med. 2011; 364: 985-7.
2. Hanahan D, Weinberg RA. The Hallmarks of Cancer. Cell. 2000; 100: 57-70.
3. Siegel RL, Miller KD, Jemal A. Cancer Statistics, 2016. CA-Cancer J Clin. 2016; 66: 7-30.
4. Shi J, Kantoff PW, Wooster R, Farokhzad OC. Cancer Nanomedicine: Progress, Challenges and Opportunities. Nat Rev Cancer. 2017; 17: 20-37.
5. Minchinton AI, Tannock IF. Drug Penetration in Solid Tumours. Nat Rev Cancer. 2006; 6: 583-92.
6. Kim KH, Jelovac D, Armstrong DK, Schwartz B, Weil SC, Schweizer C, et al. Phase 1b Safety Study of Farletuzumab, Carboplatin and Pegylated Liposomal Doxorubicin in Patients with Platinum-sensitive Epithelial Ovarian Cancer. Gynecol Oncol. 2016; 140: 210-4.
7. McMeekin S, Dizon D, Barter J, Scambia G, Manzyuk L, Lisyanskaya A, et al. Phase III Randomized Trial of Second-line Ixabepilone Versus Paclitaxel or Doxorubicin in Women with Advanced Endometrial Cancer. Gynecol Oncol. 2015; 138: 18-23.
8. Hu Q, Sun W, Wang C, Gu Z. Recent Advances of Cocktail Chemotherapy by Combination Drug Delivery Systems. Adv Drug Deliv Rev. 2016; 98: 19-34.
9. Wu H, Jin H, Wang C, Zhang Z, Ruan H, Sun L, et al. Synergistic Cisplatin/Doxorubicin Combination Chemotherapy for Multidrug-Resistant Cancer via Polymeric Nanogels Targeting Delivery. ACS Appl Mater Interfaces. 2017; 9: 9426-36.
10. Jamieson ER, Lippard SJ. Structure, Recognition, and Processing of Cisplatin-DNA Adducts. Chem Rev. 1999; 99: 2467-98.
11. Eder JP, Jr., Chan VTW, Ng S-W, Rizvi NA, Zacharoulis S, Teicher BA, et al. DNA Topoisomerase II alpha Expression is Associated with Alkylating Agent Resistance. Cancer Res. 1995; 55: 6109-16.
12. Li M, Tang Z, Lv S, Song W, Hong H, Jing X, et al. Cisplatin Crosslinked pH-sensitive Nanoparticles for Efficient Delivery of Doxorubicin. Biomaterials. 2014; 35: 3851-64.
13. Ashley CE, Carnes EC, Phillips GK, Padilla D, Durfee PN, Brown PA, et al. The Targeted Delivery of Multicomponent Cargos to Cancer Cells by Nanoporous Particle-supported Lipid Bilayers. Nat Mater. 2011; 10: 389-97.
14. Lee SM, O'Halloran TV, Nguyen ST. Polymer-caged Nanobins for Synergistic Cisplatin-doxorubicin Combination Chemotherapy. J Am Chem Soc. 2010; 132: 17130-8.
15. Pardoll D, Allison J. Cancer Immunotherapy: Breaking the Barriers to Harvest the Crop. Nat Med. 2004; 10: 887-92.
16. Lotfi-Jam K, Carey M, Jefford M, Schofield P, Charleson C, Aranda S. Non Pharmacologic Strategies for Managing Common Chemotherapy Adverse Effects: A Systematic Review. J Clin Oncol. 2008; 26: 5618-29.
17 Lancet JE, Cortes JE, Hogge DE, Tallman MS, Kovacsovics TJ, Damon LE, et al. Phase 2 trial of CPX-351, a fixed 5:1 molar ratio of cytarabine/daunorubicin, vs cytarabine/daunorubicin in older adults with untreated AML. Blood. 2014; 123: 3239-46.
18. Peer D, Karp JM, Hong S, FaroKhzad OC, Margalit R, Langer R. Nanocarriers as an Emerging Platform for Cancer Therapy. Nat Nanotechnol. 2007; 2: 751-60.
19. Ma L, Kohli M, Smith A. Nanoparticles for Combination Drug Therapy. ACS Nano. 2013; 7: 9518-25.
20. Wang C, Xu L, Liang C, Xiang J, Peng R, Liu Z. Immunological Responses Triggered by Photothermal Therapy with Carbon Nanotubes in Combination with Anti-CTLA-4 Therapy to Inhibit Cancer Metastasis. Adv Mater. 2014; 26: 8154-62.
21. Chen Q, Xu L, Liang C, Wang C, Peng R, Liu Z. Photothermal Therapy with Immune-adjuvant Nanoparticles Together with Checkpoint Blockade for Effective Cancer Immunotherapy. Nat Commun. 2016; 7: 13193.
22. Zhang L, Su H, Cai J, Cheng D, Ma Y, Zhang J, et al. A Multifunctional Platform for Tumor Angiogenesis-Targeted Chemo-Thermal Therapy Using Polydopamine-Coated Gold Nanorods. ACS Nano. 2016; 10: 10404-17.
23. Song XR, Wang X, Yu SX, Cao J, Li SH, Li J, et al. Co(9) Se(8) Nanoplates as a New Theranostic Platform for Photoacoustic/magnetic Resonance Dual-modal-imaging-guided Chemo-photothermal Combination Therapy. Adv Mater. 2015; 27: 3285-91.
24. Tian W, Su Y, Tian Y, Wang S, Su X, Liu Y, et al. Periodic Mesoporous Organosilica Coated Prussian Blue for MR/PA Dual-Modal Imaging-Guided Photothermal-Chemotherapy of Triple Negative Breast Cancer. Adv Sci. 2017; 4: 1600356.
25. Kemp JA, Shim MS, Heo CY, Kwon YJ. "Combo" Nanomedicine: Co-delivery of Multi-modal Therapeutics for Efficient, Targeted, and Safe Cancer Therapy. Adv Drug Deliv Rev. 2016; 98: 3-18.
26. Weissleder R, Ntziachristos V. Shedding Light onto Live Molecular Targets. Nat Med. 2003; 9: 123-8.
27. Liu Y, Zhi X, Yang M, Zhang J, Lin L, Zhao X, et al. Tumor-triggered Drug Release from Calcium Carbonate-encapsulated Gold Nanostars for Near-infrared Photodynamic/photothermal Combination Antitumor Therapy. Theranostics. 2017; 7: 1650-62.
28. Zhao H, Chao Y, Liu J, Huang J, Pan J, Guo W, et al. Polydopamine Coated Single-Walled Carbon Nanotubes as a Versatile Platform with Radionuclide Labeling for Multimodal Tumor Imaging and Therapy. Theranostics. 2016; 6: 1833-43.
29. Yin F, Hu K, Chen Y, Yu M, Wang D, Wang Q, et al. SiRNA Delivery with PEGylated Graphene Oxide Nanosheets for Combined Photothermal and Genetherapy for Pancreatic Cancer. Theranostics. 2017; 7: 1133-48.
30. Xing H, Hwang K, Lu Y. Recent Developments of Liposomes as Nanocarriers for Theranostic Applications. Theranostics. 2016; 6: 1336-52.
31. Yuge R, Nihey F, Toyama K, Yudasaka M. Preparation and Characterization of Newly Discovered Fibrous Aggregates of Single-Walled Carbon Nanohorns. Adv Mater. 2016; 28: 7174-7.
32. Kobayashi H, Watanabe R, Choyke PL. Improving Conventional Enhanced Permeability and Retention (EPR) Effects; What Is the Appropriate Target? Theranostics. 2013; 4: 81-9.
33. Maeda H. Toward a Full Understanding of the EPR Effect in Primary and Metastatic Tumors as well as Issues Related to Its Heterogeneity. Adv Drug Deliv Rev. 2015; 91: 3-6.
34. Perrault SD, Walkey C, Jennings T, Fischer HC, Chan WCW. Mediating Tumor Targeting Efficiency of Nanoparticles Through Design. Nano Lett. 2009; 9: 1909-15.
35. Weber J, Beard PC, Bohndiek SE. Contrast Agents for Molecular Photoacoustic Imaging. Nat Methods. 2016; 13: 639-50.
36. Wang S, Lin J, Wang T, Chen X, Huang P. Recent Advances in Photoacoustic Imaging for Deep-Tissue Biomedical Applications. Theranostics. 2016; 6: 2394-413.
37. Chen D, Wang C, Nie X, Li S, Li R, Guan M, et al. Photoacoustic Imaging Guided Near-Infrared Photothermal Therapy Using Highly Water-Dispersible Single-Walled Carbon Nanohorns as Theranostic Agents. Adv Funct Mater. 2014; 24: 6621-8.
38. Cheon YA, Bae JH, Chung BG. Reduced Graphene Oxide Nanosheet for Chemo-photothermal Therapy. Langmuir. 2016; 32: 2731-6.
39. Liu Z, Fan AC, Rakhra K, Sherlock S, Goodwin A, Chen X, et al. Supramolecular Stacking of Doxorubicin on Carbon Nanotubes for In Vivo Cancer Therapy. Angew Chem Int Edit. 2009; 48: 7668-72.
40. Liu J-H, Cao L, Luo PG, Yang S-T, Lu F, Wang H, et al. Fullerene-Conjugated Doxorubicin in Cells. ACS Appl Mater Interfaces. 2010; 2: 1384-9.
41. Wang D, Ren Y, Shao Y, Meng L. Multifunctional Polyphosphazene-coated Multi-Walled Carbon Nanotubes for the Synergistic Treatment of Redox-responsive Chemotherapy and Effective Photothermal Therapy. Polym Chem. 2017; 8: 6938-42.
42. Zhang M, Wang W, Wu F, Yuan P, Chi C, Zhou N. Magnetic and Fluorescent Carbon Nanotubes for Dual Modal Imaging and Photothermal and Chemo-therapy of Cancer Cells in Living Mice. Carbon. 2017; 123: 70-83.
43. Setua S, Ouberai M, Piccirillo SG, Watts C, Welland M. Cisplatin-tethered Gold Nanospheres for Multimodal Chemo-radiotherapy of Glioblastoma. Nanoscale. 2014; 6: 10865-73.
44. Comenge J, Sotelo C, Romero F, Gallego O, Barnadas A, Garcia-Caballero Parada T, et al. Detoxifying Antitumoral Drugs via Nanoconjugation: The Case of Gold Nanoparticles and Cisplatin. PLoS One. 2012; 7: e47562.
45. Zhu J, Liao L, Bian X, Kong J, Yang P, Liu B. pH-Controlled Delivery of Doxorubicin to Cancer Cells, Based on Small Mesoporous Carbon Nanospheres. Small. 2012; 8: 2715-20.
46. Tredan O, Galmarini CM, Patel K, Tannock IF. Drug Resistance and the Solid Tumor Microenvironment. JNCI-J Natl Cancer Inst. 2007; 99: 1441-54.
47. Turley SJ, Cremasco V, Astarita JL. Immunological Hallmarks of Stromal Cells in the Tumour Microenvironment. Nat Rev Immunol. 2015; 15: 669-82.
48. Ali-Boucetta H, Al-Jamal KT, McCarthy D, Prato M, Bianco A, Kostarelos K. Multiwalled Carbon Nanotube-doxorubicin Supramolecular Complexes for Cancer Therapeutics. Chem Commun. 2008: 459-61.
49. Yang X, Zhang X, Liu Z, Ma Y, Huang Y, Chen Y. High-Efficiency Loading and Controlled Release of Doxorubicin Hydrochloride on Graphene Oxide. J Phys Chem C. 2008; 112: 17554-8.
50. Chen W, Ouyang J, Liu H, Chen M, Zeng K, Sheng J, et al. Black Phosphorus Nanosheet-Based Drug Delivery System for Synergistic Photodynamic/Photothermal/Chemotherapy of Cancer. Adv Mater. 2017; 29: 1603864-70.
51. Bonapace L, Coissieux M-M, Wyckoff J, Mertz KD, Varga Z, Junt T, et al. Cessation of CCL2 Inhibition Accelerates Breast Cancer Metastasis by Promoting Angiogenesis. Nature. 2014; 515:130-133.
52. Wagenblast E, Soto M, Gutierrez-Angel S, Hartl CA, Gable AL, Maceli AR, et al. A Model of Breast Cancer Heterogeneity Reveals Vascular Mimicry as a Driver of Metastasis. Nature. 2015; 520: 358–362.
53. Karousis N, Suarez-Martinez I, Ewels CP, Tagmatarchis N. Structure, Properties, Functionalization, and Applications of Carbon Nanohorns. Chem Rev. 2016; 116: 4850-83.
54. McConkey DJ, Choi W, Shen Y, Lee IL, Porten S, Matin SF, et al. A Prognostic Gene Expression Signature in the Molecular Classification of Chemotherapy-naive Urothelial Cancer is Predictive of Clinical Outcomes from Neoadjuvant Chemotherapy: A Phase 2 Trial of Dose-dense Methotrexate, Vinblastine, Doxorubicin, and Cisplatin with Bevacizumab in Urothelial Cancer. Eur Urol. 2016; 69: 855-62.

55. Liao L, Liu J, Dreaden EC, Morton SW, Shopsowitz KE, Hammond PT, et al. A Convergent Synthetic Platform for Single-Nanoparticle Combination Cancer Therapy: Ratiometric Loading and Controlled Release of Cisplatin, Doxorubicin, and Camptothecin. J Am Chem Soc. 2014; 136: 5896-9.
56. Park JH, von Maltzahn G, Xu MJ, Fogal V, Kotamraju VR, Ruoslahti E, et al. Cooperative Nanomaterial System to Sensitize, Target, and Treat Tumors. Proc Natl Acad Sci U S A. 2010; 107: 981-6.
57. Wang Y, Wang K, Zhao J, Liu X, Bu J, Yan X, et al. Multifunctional Mesoporous Silica-coated Graphene Nanosheet Used for Chemo-photothermal Synergistic Targeted Therapy of Glioma. J Am Chem Soc. 2013; 135: 4799-804.
58. Robinson JT, Tabakman SM, Liang Y, Wang H, Casalongue HS, Vinh D, et al. Ultrasmall Reduced Graphene Oxide with High Near-infrared Absorbance for Photothermal Therapy. J Am Chem Soc. 2011; 133: 6825-31.
59. Zha Z, Yue X, Ren Q, Dai Z. Uniform Polypyrrole Nanoparticles with High Photothermal Conversion Efficiency for Photothermal Ablation of Cancer Cells. Adv Mater. 2013; 25: 777-82.
60. Thigpen JT, Brady MF, Homesley HD, Malfetano J, DuBeshter B, Burger RA, et al. Phase III trial of Doxorubicin With or Without Cisplatin in Advanced Endometrial Carcinoma: A Gynecologic Oncology Group Study. J Clin Oncol. 2004; 22: 3902-8.
61. Liang C, Diao S, Wang C, Gong H, Liu T, Hong G, et al. Tumor Metastasis Inhibition by Imaging-guided Photothermal Therapy with Single-Walled Carbon Nanotubes. Adv Mater. 2014; 26: 5646-52.
62. Duan X, Chan C, Guo N, Han W, Weichselbaum RR, Lin W. Photodynamic Therapy Mediated by Nontoxic Core-Shell Nanoparticles Synergizes with Immune Checkpoint Blockade To Elicit Antitumor Immunity and Antimetastatic Effect on Breast Cancer. J Am Chem Soc. 2016; 138: 16686-95.
63. Yu X, Gao D, Gao L, Lai J, Zhang C, Zhao Y, et al. Inhibiting Metastasis and Preventing Tumor Relapse by Triggering Host Immunity with Tumor-Targeted Photodynamic Therapy Using Photosensitizer-Loaded Functional Nanographenes. ACS Nano. 2017; 11: 10147-58.
64. Wang D, Wang T, Liu J, Yu H, Jiao S, Feng B, et al. Acid-Activatable Versatile Micelleplexes for PD-L1 Blockade-Enhanced Cancer Photodynamic Immunotherapy. Nano Lett. 2016; 16: 5503-13.
65. Yu M, Zheng J. Clearance Pathways and Tumor Targeting of Imaging Nanoparticles. ACS Nano. 2015; 9: 6655-74.
66. Li SD, Huang L. Pharmacokinetics and Biodistribution of Nanoparticles. Mol Pharm. 2008; 5: 496-504.
67. Sykes EA, Chen J, Zheng G, Chan WC. Investigating the Impact of Nanoparticle Size on Active and Passive Tumor Targeting Efficiency. ACS Nano. 2014; 8: 5696-706.
68. Zhang Z, Wang J, Nie X, Wen T, Ji Y, Wu X, et al. Near Infrared Laser-induced Targeted Cancer Therapy Using Thermoresponsive Polymer Encapsulated Gold Nanorods. J Am Chem Soc. 2014; 136: 7317-26.
69. Yang Y, Zhang L, Cai J, Li X, Cheng D, Su H, et al. Tumor Angiogenesis Targeted Radiosensitization Therapy Using Gold Nanoprobes Guided by MRI/SPECT Imaging. ACS Appl Mater Interfaces. 2016; 8: 1718-32.
70. Chou T-C, Talalay P. Quantitative Analysis of Dose-effect Relationships: The Combined Effects of Multiple Drugs or Enzyme Inhibitors. Adv Enzyme Regul. 1984; 22: 27-55.
71. Shen D-W, Pouliot LM, Hall MD, Gottesman MM. Cisplatin Resistance: A Cellular Self-Defense Mechanism Resulting from Multiple Epigenetic and Genetic Changes. Pharmacol Rev. 2012; 64: 706-21.
72 Li Y, Liu G, Ma J, Lin J, Lin H, Su G, et al. Chemotherapeutic drug-photothermal agent co-self-assembling nanoparticles for near-infrared fluorescence and photoacoustic dual-modal imaging-guided chemo-photothermal synergistic therapy. J Control Release. 2017; 258: 95-107.
73. Wang J, Xie Y, Wang L, Tang J, Li J, Kocaefe D, et al. In Vivo Pharmacokinetic Features and Biodistribution of Star and Rod Shaped Gold Nanoparticles by Multispectral Optoacoustic Tomography. RSC Adv. 2015; 5: 7529-38.
74. Morscher S, Driessen WHP, Claussen J, Burton NC. Semi-quantitative Multispectral Optoacoustic Tomography (MSOT) for Volumetric PK Imaging of Gastric Emptying. Photoacoustics. 2014; 2: 103-10.
75. Rui Y-P, Liang B, Hu F, Xu J, Peng Y-F, Yin P-H, et al. Ultra-large-scale Production of Ultrasmall Superparamagnetic Iron Oxide Nanoparticles for T1-weighted MRI. RSC Adv. 2016; 6: 22575-85.